

Tamara Janz

Cloud formation on tidally locked exoplanets with a F-type host star

BACHELOR'S THESIS

to achieve the university degree of
Bachelor's degree programme: Physics

submitted to

Graz University of Technology

Supervisor

Prof. Dr.rer.nat. Christiane Helling,
Institut für Theoretische Physik - Computational Physics

Co-Supervisor

MSc. Sven Kiefer,
OEAW

Graz, June 2024

Abstract

This thesis analyses the cloud formation on exoplanets, which orbit a star in a system different and far away from our solar system. The focus here is on systems with a F-type host star, a star hotter and brighter than our sun with an effective temperature of 6550 K. Due to its brightness, it is easier to observe whether planets are orbiting it. The exoplanets are tidally locked, which causes a strong contrast between the side of the planet facing the star and the side facing away from the star. The cloud simulation is modelled using the *StaticWeather* model by Voitke and Helling (2003) and the dataset from hot Jupiters with an equilibrium temperature of $T_{eq} = 1400$ K up to a temperature of $T_{eq} = 2600$ K compiled by a 3D General Circulation Model (GCM) by Schneider et al. (2022). This report compares the cloud formation on a $T_{eq} = 2600$ K exoplanet with the cloud formation on a $T_{eq} = 1800$ K exoplanet. The differences between the two mixing types (normal and scaled) and the two versions of GCM (old and new) are also explained. Another comparison mentioned in this thesis is that of the pressure course compiled by the older version of the GCM and the new version of the GCM. It turns out that the equilibrium temperature, the associated distance to the star, as well as the mixing type make a huge impact on the cloud structures. The clouds simulated by a normal mixed model have a greater mean particle size than the clouds simulated by the scaled mixed model. Exoplanets with a high equilibrium temperature only form clouds on the side facing away from the star, while the clouds on exoplanets with a lower equilibrium temperature can form globally.

Contents

1	Introduction	2
1.1	Equilibrium and effective temperature	3
1.2	Cloud formation process	3
1.3	3D General Circulation Model	4
1.4	Motivation	4
2	Methods	5
2.1	Cloud formation modeling	5
2.2	Comparison of the two GCMs	6
2.3	Two mixing timescales	6
2.4	Generation of cloud simulations	7
3	Results	9
3.1	Comparison of the two GCM models	9
3.2	Comparison of the mixing efficiencies	11
3.3	Simulations of the cloud structure	13
3.3.1	Planets with an equilibrium temperature of 2600 K	14
3.3.2	Planets with an equilibrium temperature of 1800 K	20
4	Discussion	26
4.1	Comparison of the GCM models	26
4.2	Difference between normal and scaled mixing	26
4.3	Intercomparison of planets	27
5	Conclusion	28
5.1	Outlook	29

Chapter 1

Introduction

As of this date (June 2024), 5905 diverse exoplanets are known to exist¹. Because of this diversity, space missions such as PLATO (launch 2027) have the goal to characterise exoplanets and search for 'planetary transits'. The first step for future space travel is to determine whether a planet has an atmosphere. This can be verified by certain chemical composition and by the existence of gaseous species (eg. H₂O, AlO, CrH). If the planet has an atmosphere, it is important to know what the cloud structure looks like for later observations of this planet. This thesis is about the atmospheres on tidally locked exoplanetary hot Jupiters, focusing on the cloud formation in those atmospheres.

Hot Jupiters are exoplanets with a mass roughly equal to or greater than that of Jupiter and whose surface temperature is significantly higher. Due to their large diameter, they are easier to find through the transit method. This method is a procedure for the detection of exoplanets in which the brightness of a star is measured as the planet passes in front of the star.

The exoplanets depicted in this thesis are also tidally locked. Their rotation around the host star takes them as long as to rotate around their own axis. Here they rotate around a F-type hosts star, which is larger and brighter than our sun, with an effective temperature of $T_{eff} = 6550$ K.

¹<https://exoplanet.eu/home/>

1.1 Equilibrium and effective temperature

The effective temperature of a star is the temperature of a black body, which has the same luminous intensity.

Because of the temperature changes on the exoplanet (day and night side) the effective temperature is not clear. For this reason, the equilibrium temperature T_{eq} is used for planets.

In the paper by Koll (2022) the equilibrium temperature T_{eq} is established as

$$T_{eq} = T_* \sqrt{\frac{R_*}{2d}} (1 - \alpha_B)^{1/4} \quad (1.1)$$

With T_* as the stellar temperature, R_* as the stellar radius, d as the planetary semi-major axis and α_B as the planet's bond albedo. In this case, the measure for the reflectivity, the albedo, is set to 0, because reflection is not taken into account. Koll (2022) also associates T_{eq} with the temperature of the day side of the observed planet T_{day} :

$$T_{day} = (4f)^{1/4} T_{eq} \quad (1.2)$$

Here f is the heat redistribution factor, which lies between $\frac{2}{3}$ and $\frac{1}{4}$. Here $\frac{1}{4}$ was chosen.

1.2 Cloud formation process

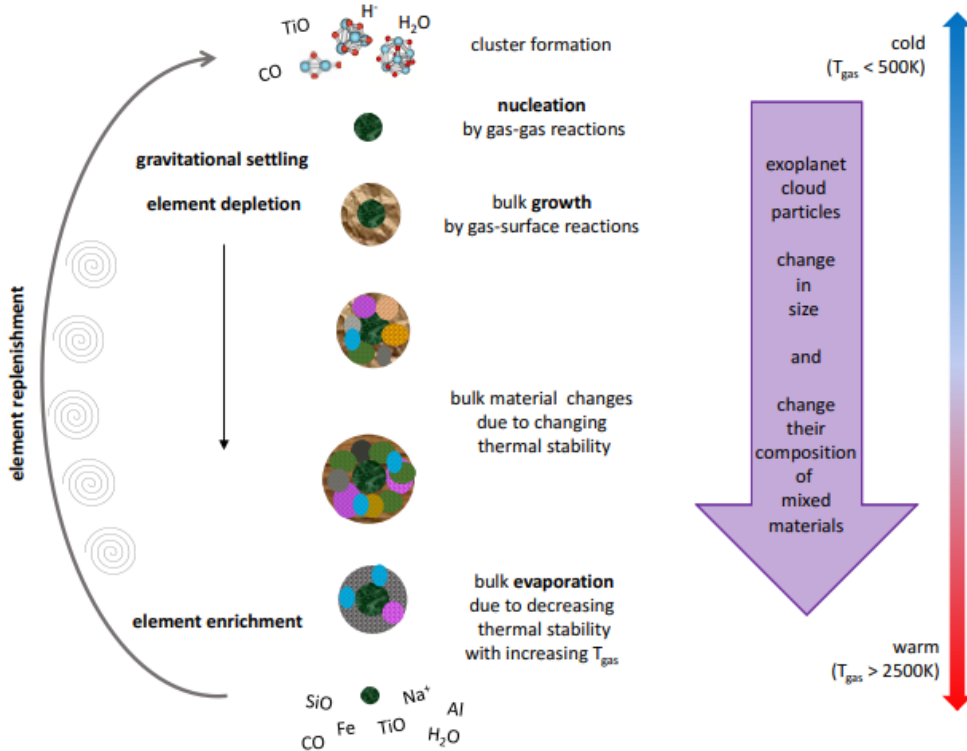


Figure 1.1: Cloud formation process. Image taken from Helling (2019)

Like described in the papers Helling (2019), Helling (2021) and Helling (2022), the formation of clouds begins in the gas phase high up in the atmosphere of the planet. Here nucleation happens, condensation seeds are formed through gas-gas reactions. Due to the gravitation of the planet those particles fall deeper into the atmosphere. On their way down the bulk of the cloud particle grows in mass by gas-surface reactions. They also collide with other material that can condensate onto the particle if the thermal conditions are right. The particles settle into the deeper atmosphere, where the pressure and the temperature are higher. Here they may coagulate to form larger particles or they shatter due to particle-particle collisions. Even deeper in the atmosphere the temperatures are so high that the cloud particles evaporate. Through element replenishment the remaining individual elements are brought back to the higher atmosphere to repeat this cycle.

Unlike on earth the clouds in hot Jupiter atmospheres do not consist of water, which would evaporate in the high temperature there. Because of this these clouds in the atmosphere consists of solid materials. The cloud nucleation species TiO_2 and SiO (also NaCl , KCl) are located in the very top layers of the atmosphere. In the middle area of the cloud layer materials made of a mix of Mg/Fe/Si/O and Ca/Al can be found. In even deeper layers, where the temperature is higher, the clouds are made of Fe[s] , $\text{Al}_2\text{O}_3[\text{s}]$ and $\text{CaTiO}_3[\text{s}]$ (Helling, 2022).

1.3 3D General Circulation Model

For the simulation of the cloud formation in exoplanetary atmospheres 3D General Circulation Models (GCM) are used. Inside this model the impact of stellar irradiation and the material transport are calculated for each vertical profile (Schneider et al., 2022). Also the mass, momentum and energy conservation equation is solved to calculate the local temperature, the local density, the gas pressure and the local velocity field of the gas that makes up the atmosphere. The compiled data is than used further for the modeling of the cloud structure, which happens outside the GCM.

1.4 Motivation

The goal of this thesis is to compare the cloud formation on exoplanets near their F-type host star and the cloud formation on exoplanets further away from their host star. The thesis further investigates the effect of the mixing timescale on the cloud structure. It could be possible to create a 3D GCM in which the cloud formation process is directly incorporated with the knowledge of how to solve the calculations for the cloud simulation and the general behaviour of the clouds in certain exoplanetary atmospheres in F-type star systems.

Chapter 2

Methods

2.1 Cloud formation modeling

To simulate the clouds on exoplanets the *StaticWeather* model by Woitke and Helling (2003) is used (see also Woitke and Helling, 2004; Helling and Woitke, 2006; Helling et al., 2008). It sets the conditions of a plane-parallel atmosphere geometry, where the gas velocity v_{gas} as well as the dust moments $\frac{\partial L_j}{\partial t}$ are set to 0. Because a static stationary atmosphere must remain cloud free (Woitke and Helling, 2004), the convective mixing timescale τ_{mix} is introduced.

The convective mixing timescale τ_{mix} [s] can be obtained through the following equation (Helling et al. (2023), Appendix B):

$$\tau_{mix} = \int_0^z \frac{1}{v(z')} dz' \quad (2.1)$$

whereby z [cm] is the distance and $v(z')$ [cm/s] the velocity.

The cloud formation modeling starts with modelling the formation of the condensation seeds. Here the kinetic, steady-state approach is used. The temporal evolution of the cluster size distribution function $f(N, t)$ is described as (Helling, 2022):

$$\frac{df(N, t)}{dt} = \sum_{i=1}^I J_i^C(N, t) - \sum_{i=1}^I J_i^C(N + i, t) \quad (2.2)$$

with $f(N)$ as the number density of a molecular cluster with N i -mers and $J_i^C(N, t)$ as the effective flux.

For the modelling of the the bulk growth of cloud particles the dust moment equation for the cloud particle size distribution $f(V)$ [cm⁻⁶] is solved (Helling, 2022).

$$\frac{\partial}{\partial t}(f(V)dV) + \nabla \cdot (v_d(V)f(V)dV) = \sum_k R_k dV \quad (2.3)$$

Here the cloud particle velocity is the sum of the local gas velocity and the relative velocity: $v_d(V) = v_{gas} + v_{dr}(V)$. R_k are the various surface chemical reactions

(Helling and Woitke, 2006). A precise solution approach for equation 2.2 and 2.3 can be found in Helling (2022).

With the dust moments $L_j(x, t)$ [cm^j/g] ($j = 0, 1, 2$) defined as (Helling and Woitke, 2006):

$$\rho L_j(x, t) = \int_{V_l}^{\infty} f(V, x, t) V^{j/3} dV \quad (2.4)$$

where V_l [cm^3] is the minimum volume of a cluster, cloud properties can be expressed (Helling, 2022):

- cloud particle number density: $n_d = \rho L_0$
- mean particle size: $\langle a \rangle = \sqrt[3]{\frac{3}{4\pi}} \cdot \frac{L_1}{L_0}$
- mean particle surface: $\langle A \rangle = \sqrt[3]{36\pi} \cdot \frac{L_2}{L_0} = A_{cloud}^{tot}/n_d$
- mean particle volume: $\langle V \rangle = \frac{L_3}{L_0} = \sum V_s$ with $V_s = \frac{L_3^s}{L_0}$

2.2 Comparison of the two GCMs

This thesis includes a comparison between the data in the 3D General Circulation Model (GCM) obtained by an older version of code by Baeyens et al. (2022) and by a newer version by Schneider et al. (2022). The difference between those two models is that in the older version there is no radiative transfer. In the older model a 1D pressure-temperature T_{eq} profile and radiative time scale τ_{rad} for every grid point on the planet is calculated outside the GCM. The grid points have a dimension of 32x32x6 horizontal cells times 47 vertical cells. The two parameters T_{eq} and τ_{rad} are then called by the 3D GCM and used during the 'Newtonian cooling' (see also Carone et al., 2020; Baeyens et al., 2021, 2022). In the new model the radiative transfer is fully calculated inside the 3D GCM for each vertical profile with the inclusion of the material transport (Schneider et al., 2022).

In those GCMs the global parameters such as the planetary equilibrium temperature for F stars as planetary host stars can be found. This data was created and provided by Dr. Ludmila Carone. To see the difference between these two data sets clearer, a line plot of the pressure course at the longitudes 0° (sub stellar point), 90° (evening terminator), 180° (anti stellar point) and -90° (morning terminator) with a latitude of 0° is created and shown in figure 3.1.

It should be mentioned, that in this thesis for the cloud simulations the data from the 3D GCM model grid of the newer version is used.

2.3 Two mixing timescales

To get a better understanding of the impact of the mixing timescale, there is a comparison between two mixing timescales. This parameter describes how fast the

material is returned to the upper layer of the atmosphere after the vaporisation in the deeper layers. For the scaled mixing the timescale is multiplied by the factor 10^{-2} , for the normal mixing by the factor 1.

Additionally to the slice plots showing the gas temperature course, the nucleation rate, the dust-to-gas ratios and the mean particle size in a 3D model, 1D plots are also created for both types of mixing. In these 1D plots the same distributions are plotted with the addition of the mixing timescale itself.

2.4 Generation of cloud simulations

For a better understanding on how the temperature is distributed on the planet, what is the relation between the particle density and the general density, the mean size of the particles in the regions of the planet and the course of nuclei there are slice plots, which show these distributions.

For each planet, the results are visualised by eight slice plots, whereby four plots depict the equatorial plane and the other four describe the terminator plane. Each of the previous mentioned distributions is represented for both slice plots.

The values of longitude, latitude, gas pressure, gas temperature and gas velocity of the selected planet are all stored in a GCM file, which has .nc as data type. However the code, which is used for generate the profiles of the planet, is made to use the .data as data type. So for the first step, the .nc file is converted to the text file .data with the python script *StaticWeather Multirun* by Dr. Dominic Samra.

The new transformed file is used as an input for the *StaticWeather Multirun*, as well is the equilibrium temperature of the selected planet. Also the tolerance, the maximum run time and the scaling factor have to be pasted. The tolerance of the ODE solver is, for most of the runs, set to 10^{-5} , while the maximum run time is either 1200 seconds or 7200 seconds. The maximum time determines how long four profiles run at maximum before they break up.

The scaling, a factor multiplying the mixing timescale is set to either 10^{-2} for scaled mixing or 1 for normal mixing.

This thesis depicts the planets in a solar system with a F-star, which has an effective temperature of 6550 K. This data is needed to run the code for the right planet. Also choosing the specific longitudes and latitudes, which will be shown in the slice plots of the planet.

The selected values for the longitude are: -150, -120, -90, -60, -30, 0, 30, 60, 90, 120, 150, 180

For the latitude the values are: 0, 45, 23, 68

Most parameters are declared in the first run and remain unchanged for the ones to follow. Only 'appendix' ('normal'/'scaled') and the equilibrium temperature of the currently analysed planet change regularly throughout the measurements.

This file then calls the previously adjusted file and the fortran script of *StaticWeather* by Prof. Christiane Helling and Dr. Peter Woitke to start the run. It also automates the running of multiple *StaticWeather* instances at a time. In this case it runs four profiles simultaneously for the defined maximum run time. In total 48 profiles are compiled.

To check if all profiles are finished and have not broken up throughout the process, the final pressure level of the profile is analysed. The pressure should be 650 bar, which is the inner boundary of the input (T_{gas}, p_{gas})-structures from the 3D GCM models. Whether a profile has completed the run depends on various factors, such as the time limit and the tolerance.

Besides these output folders with the data of each profile there is also a 'done' file. It indicates the complete finish of the run, 'T' (true) for a finished run, 'F' (false) for a not finished run. If the run failed and there does not exist a 'done' file, it is written down as 'NDF' (no done file).

If the runs are completed and the 'done' files of the profiles have all a 'T', the slice plots for these profiles can now be compiled. The eight created slice plots will be discussed further in the course of this paper. The individual plots are shown in section 3.3 and discussed in section 4.3.

Suggestions of changes in the execution if a profile failed

It is essential for the slice plots, that all needed profiles have to be finished ('done' file says 'T'). If one shown profile has broken off during the run, no data can be seen in the plot and the affected section remains white (see figure in chapter 5.1).

When a run of a planet is done, it sometimes happens that one or more profiles are not finished or they do not even have a done file in the output folder. If this occurs there are some measures to be taken to make sure it works on the subsequent runs.

The tolerance can be increased. Normally it is set on 10^{-7} , but it can be raised to 10^{-5} .

If the increase in tolerance does not provide any changes to the output of the run, the maximum time, which describes the time four profiles should run through at maximum, can also be increased. On the first run of a planet, the maximum time is at 1200 seconds (20 minutes), which is increased to 7200 seconds (two hours) in the case of an incomplete profile.

Chapter 3

Results

3.1 Comparison of the two GCM models

This section compares the data of the planetary atmospheres with a F-type host star obtained through an older version by Baeyens et al. (2022) and the new version by Schneider et al. (2022). Here a comparison graph with the gas pressure, p_{gas} [bar] in dependency to the gas temperature, T_{gas} [K] is plotted to show the differences in the data of the depicted longitudes of a $T_{eq} = 2600$ K planet (fig.3.1).

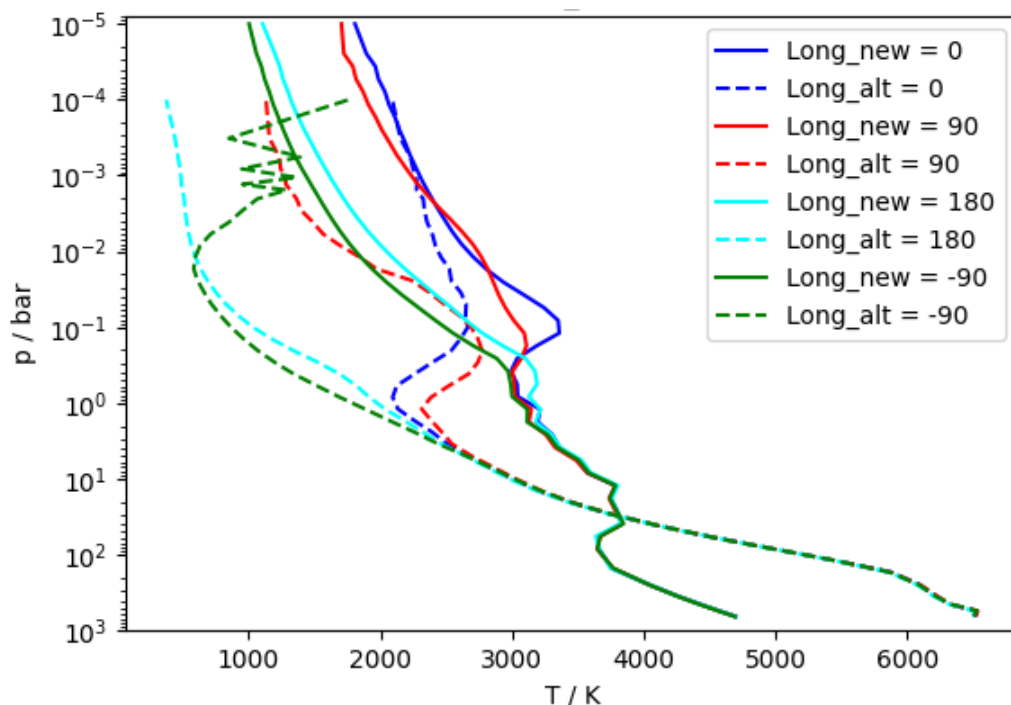


Figure 3.1: The Comparison between two 3D GCM simulations for a planet of $T_{eq} = 2600$ K orbiting an F-type host star: The older simulation model by Baeyens (dashed lines) and the new model by Schneider (solid lines) depicted at the sub stellar point (0°), evening terminator (90°), anti stellar point (180°) and at the morning terminator (-90°)

Figure 3.1 shows the pressure course of the longitudes at 0° , 90° , 180° and -90° along the temperature. The solid lines depict the data from the new model (Schneider et al., 2022), while the dashed lines follow the older model (Baeyens et al., 2022).

At about 1 bar the pressure of all longitudes by both models intertwine. But there are more differences between the two models than similarities. In general the temperature of the older version is lower than the one of the new model. For example the 180° longitude of the old model at $p_{gas} = 10^{-4}$ bar has a gas temperature under 1000 K, while the same longitude by the newer model has a temperature over 1500 K at the identical pressure. Also the data of the older model starts at $p_{gas} = 10^{-4}$ bar, the newer version starts in lower pressure.

Even the paths of the individual longitudes are different. The -90° longitude of the old model follows a zigzag line between 10^{-4} bar and 10^{-3} bar (green dashed line in fig. 3.1), whereas the new version does not. With the newer model the courses of the longitudes at 0° and 90° are close together even overlap three times above 1 bar (red and blue lines). On the other hand the same longitudes of the old model have a temperature difference of about 1000 K and overlap once before the 1 bar mark.

It is noticeable that the longitude at 0° from the new model (blue solid line) has a swing out between 3000 K and 4000 K. The longitude at 0° and 90° of the old model does so as well.

3.2 Comparison of the mixing efficiencies

For a better understanding of the differences in the normal mixed and scaled mixed model and how they influence the cloud formation process, take a look on the 1D plots (figures 3.2-3.4). In this section the 1D plots of the gas temperature course, the mixing timescale, the cloud particle number density, the mean particle size, the nucleation rate and the dust-to-gas ratio is shown. Furthermore the effects of these parameters on each other can be seen. Here is an example of an exoplanet with an equilibrium temperature of 2600 K.

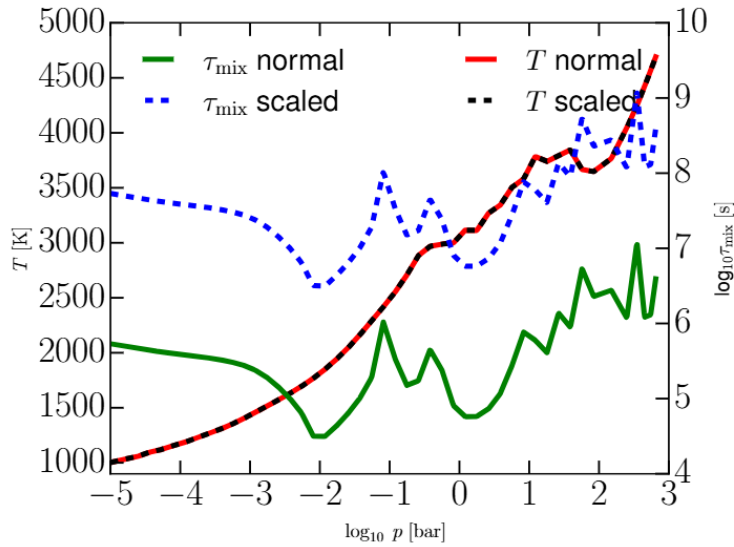


Figure 3.2: The gas temperature T_{gas} [K] and the mixing timescale τ_{mix} [s] for the normal (solid line) and the scaled mixing (dashed line) in dependence of the gas pressure p_{gas} [bar] for an exoplanet with an equilibrium temperature of 2600 K

Figure 3.2 shows the 1D plot of the gas temperature course and the mixing timescale of a $T_{eq} = 2600$ K planet in the normal mixed and in the scaled mixed model. The temperature courses do not deviate from each other, because it comes from the GCM and is used as an unchanged input for the cloud model. The courses of the timescale have a time difference by a factor of 10^2 , due to the affects of τ_{mix} on the cloud modelling routines. Whereby the scaled mixed version (blue dashed line) features the longer timescales. With the rise of the pressure the temperature becomes higher.

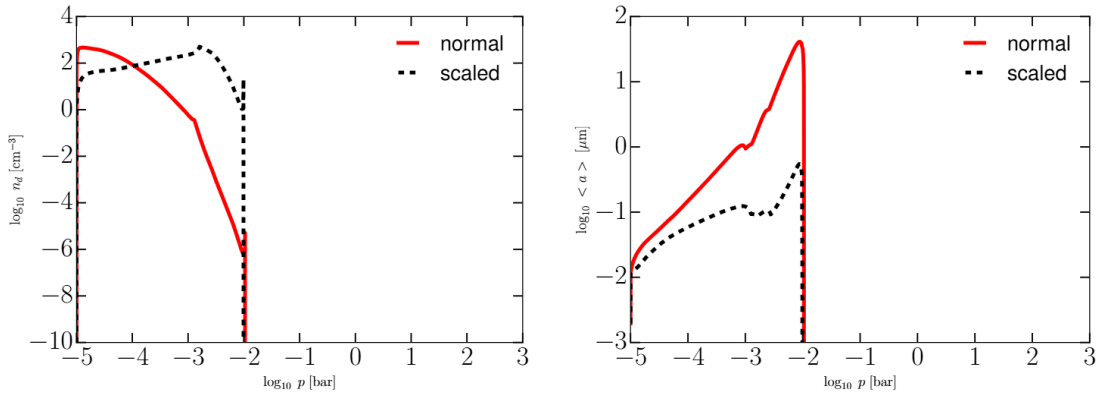


Figure 3.3: The cloud particle number density n_d [cm^{-3}] (left) and the mean particle size $\langle a \rangle$ [μm] (right) for the normal (solid line) and the reduced mixing (dashed line) in dependence of the gas pressure p_{gas} [bar] for an exoplanet with an equilibrium temperature of 2600 K

Based on the course of the particle quantity in figure 3.3 (left) its value in the normal mixed version (red line) decreases with the greater pressure. The quantity in the reduced mixed version (black dashed line) increases a little when the pressure rises, before it drops after 10^{-3} bar. At 10^{-2} bar both courses coincide. In the right graphic the mean particle size of both the normal and the scaled mixed version increase with the greater pressure, whereas the size of the normal mixed version reaches higher values. Like in the left plot the two curves coincide at 10^{-2} bar.

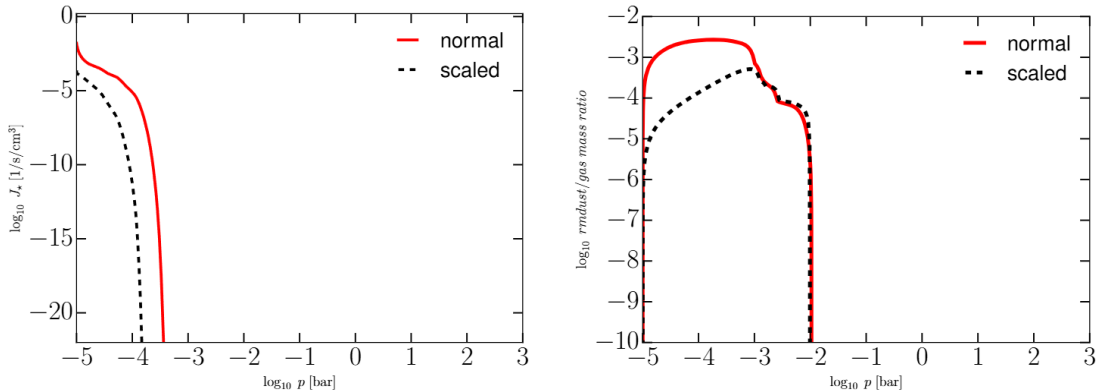


Figure 3.4: The nucleation rate J_* [$\text{cm}^{-3}\text{s}^{-1}$] (left) and the dust-to-gas ratio ρ_{dust}/ρ_{gas} (right) for the normal (solid line) and the scaled mixing (dashed line) in dependence of the gas pressure p_{gas} [bar] for an exoplanet with an equilibrium temperature of 2600 K

The nucleation rates in the left plot in figure 3.4 decrease nearly exponential the higher the pressure. In the scaled mixed version (black dashed line) the nucleation reaches zero near the 10^{-4} bar mark. In the normal mixed version (red line) nucleation stops in the middle between 10^{-4} bar and 10^{-3} bar. The right graphic shows the dust-to-gas ratio. At the beginning the curve of the normal mixed

version rises up to a bit over 10^{-3} . Here it continues at a nearly constant rate before it goes beyond 10^{-3} bar where it falls in steps and ends abruptly at 10^{-2} bar. In contrast the scaled mixed ratio starts at a lower value and increases until 10^{-3} bar is reached. Where it intertwines with the normal mixed ratio and at 10^{-2} bar abruptly stops.

3.3 Simulations of the cloud structure

As previously in section 2.4 mentioned, the generated slice plots of the respective planetary atmospheres will be shown and described in this chapter. For each planet of the equilibrium temperature, there are four equatorial slice plots and four terminator slice plots.

The equatorial slice depicts the distributions located on the equator, so the latitude angle θ is at 0° . In this case the longitudes angles ϕ range from -150° to 180° (see section 2.4). But the labels on the slice plots here depicted go from 0° to 360° (again 0°). Because the planets are tidally locked, the side which always faces the sun is called the 'day side'. The side facing away from the sun is called the 'night side'. The point on the 90° mark represents the evening terminator, the 270° mark the morning terminator.

In the terminator slice the angle of the longitude ϕ is at 90° on the right side of the vertical axis and 270° on the left side. While the latitudes θ range from 0° to 68° (see section 2.4).

Because the planet is aligned, so that the sun shines behind it, the left side represents the evening side and the right the morning side. The plot itself is mirrored via the horizontal axis. So the distributions in the north (from the plot point of view) are the same as the ones in the south.

There is also labeling of the logarithmic pressure in [bar] on the horizontal line, which ranges from a bit under 10^{-4} bar to 10^6 bar. The pressure is displayed in both kinds of slice plots.

The first slice plot depicts the gas temperature distribution in the planetary atmosphere in [K], while the second plot shows the logarithmic nucleation rate J_* in $[\text{cm}^{-3}\text{s}^{-1}]$. In the third the dust-to-gas ratio ρ_{dust}/ρ_{gas} can be seen and the last one describes the logarithmic particle size $\langle a \rangle$ in $[\mu\text{m}]$.

In each of the following figures, two slice plots are shown - one representing the normal mixing and one the scaled mixing. The difference between those mixing methods are the following: In the formation of clouds there is a step where the freshly fallen particle goes up again. With the scaled mixing this process happens slower, so that the particle needs more time to rise up. Because of this the formed nucleation seeds became less and likewise the clouds became less.

3.3.1 Planets with an equilibrium temperature of 2600 K

Gas temperature distribution

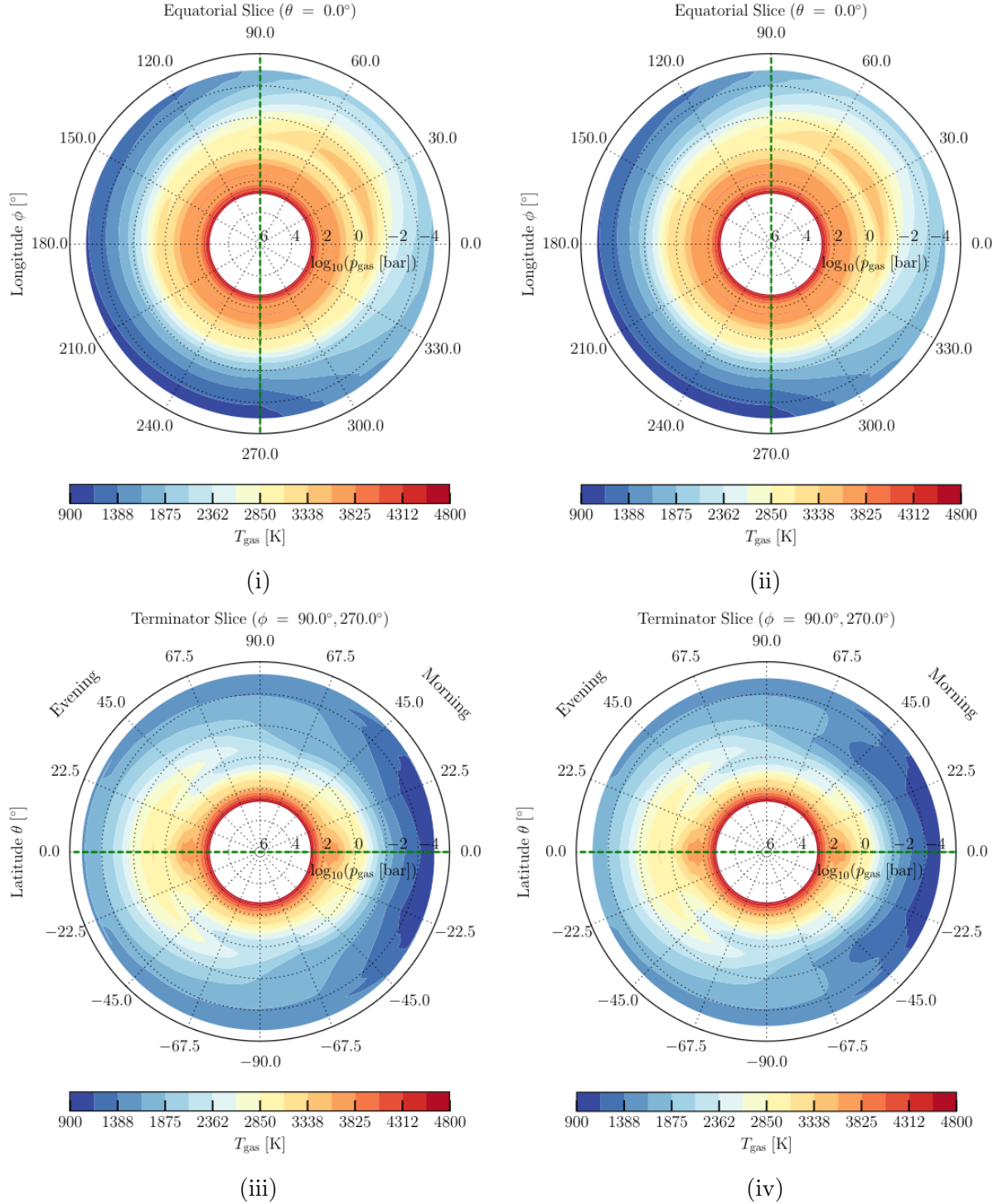


Figure 3.5: Equatorial (top) and terminator (bottom) slice plots of the gas temperature course in the atmosphere of a planet with the equilibrium temperature $T_{eq} = 2600$ K with normal (left) and scaled mixing (right)

The figure 3.5 shows the gas temperature distribution in the planetary atmosphere of a planet with a F host star at the equatorial plane. The local gas temperature ranges from 900 K to 4800 K, whereby the temperature increases the closer it reaches the center. At about 10^3 bar the maximum temperature of 4800 K is reached and below no more data can be found, as it can be seen based on the white circle.

The night side of the planet has a wider expansion of lower temperature than the morning side, as seen in the equatorial slices 3.5i and 3.5ii. A flow in temperature is noticeable since the lowest temperature of 900 K to 1154.5 K moves from 150° to over 270° (evening terminator) and the plane becomes wider with the rising longitude angle. While at the morning terminator at a pressure level of under $p_{gas} = 10^{-4}$ bar the temperature amounts 1388 K to 1631.5 K.

At $\phi = 30^\circ$ and $p_{gas} = 10^{-1}$ bar an increase in temperature can be seen in comparison to the temperatures on a lower and higher pressure level.

Figures 3.5iii and 3.5iv show the terminator slices. It can be observed that the plot is mirrored at the horizontal line (green dashed line). The temperature is much more cooler on the morning side than on the evening side. This can also be detected in the equatorial slices.

There are no difference found between the scaled and the normal mixed slice plots. More to that in the section 4.3.

Nucleation rate

The nucleation rate in the atmosphere of a $T_{eq} = 2600$ K planet is shown in figure 3.6. Nucleation mostly happens on the night side of the planet, like shown in figures 3.6i and 3.6ii. There it reaches a maximum rate of $10^{-2} \text{ cm}^{-3}\text{s}^{-1}$ for the normal mixed version and $10^{-4} \text{ cm}^{-3}\text{s}^{-1}$ as the highest rate for the scaled mixed version. Like the cold temperatures in the plots 3.5, the nucleation rate reaches over the morning terminator (270°) up to the 300° mark. Its highest reached pressure level is between 10^{-4} bar and 10^{-3} bar via normal mixing (3.6i) and only 10^{-4} bar via scaled mixing (3.6ii).

According to the figures 3.6iii and 3.6iv nucleation only happens on the morning side. Except of an outlier a little bit over 10^{-2} bar, where a low nucleation rate reaches into the evening side.

The nucleation in the normal mixed routine (3.6iii) reaches higher pressures and has higher values than the nucleation in the scaled mixed routine (3.6iv)

On a lower pressure level the nucleation rate is higher, whereas in deeper regions it decreases.

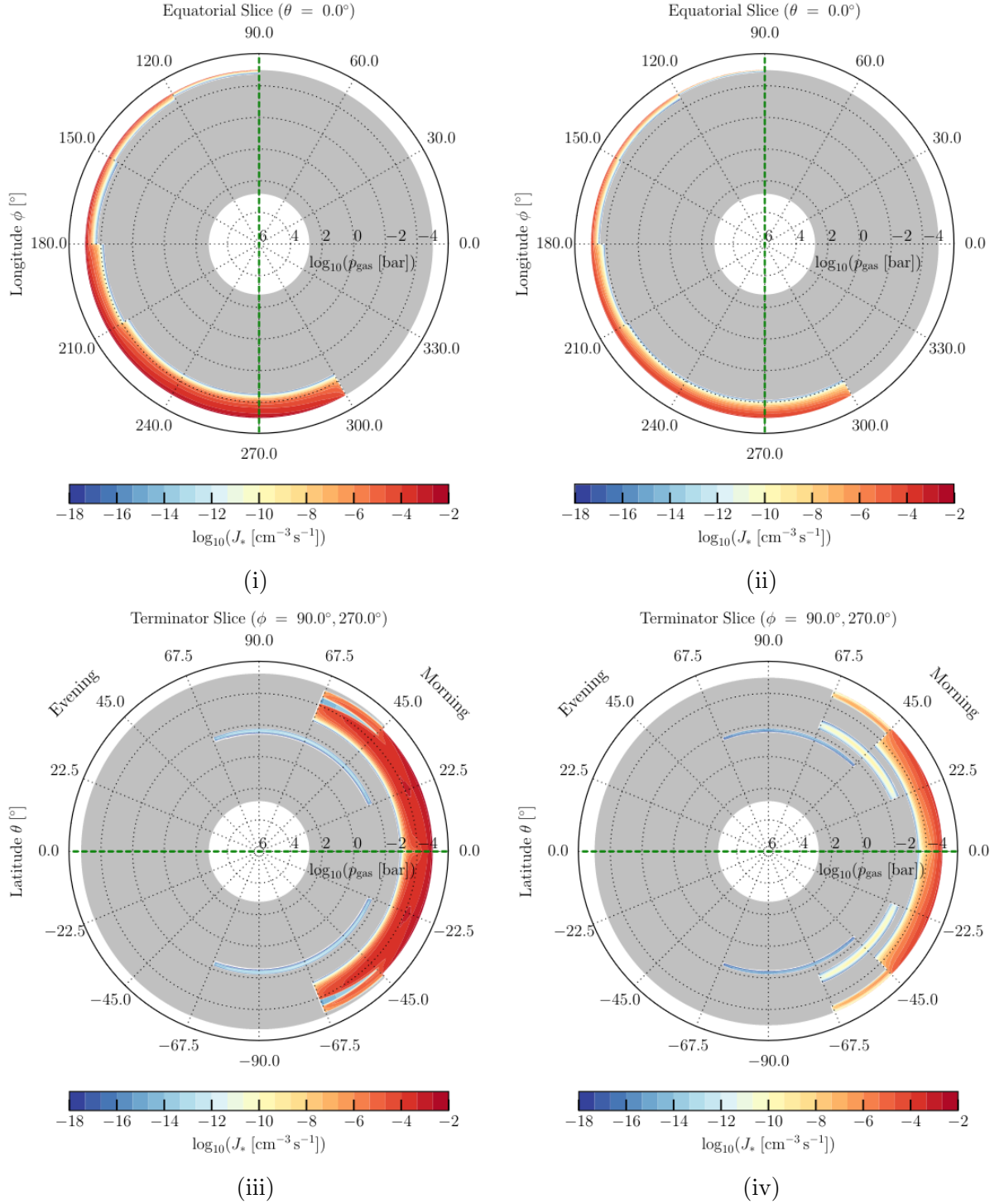


Figure 3.6: Equatorial (top) and terminator (bottom) slice plots of the nucleation rate in the atmosphere of a planet with the equilibrium temperature $T_{eq} = 2600$ K with normal (left) and scaled mixing (right)

Gas-to-dust ratios

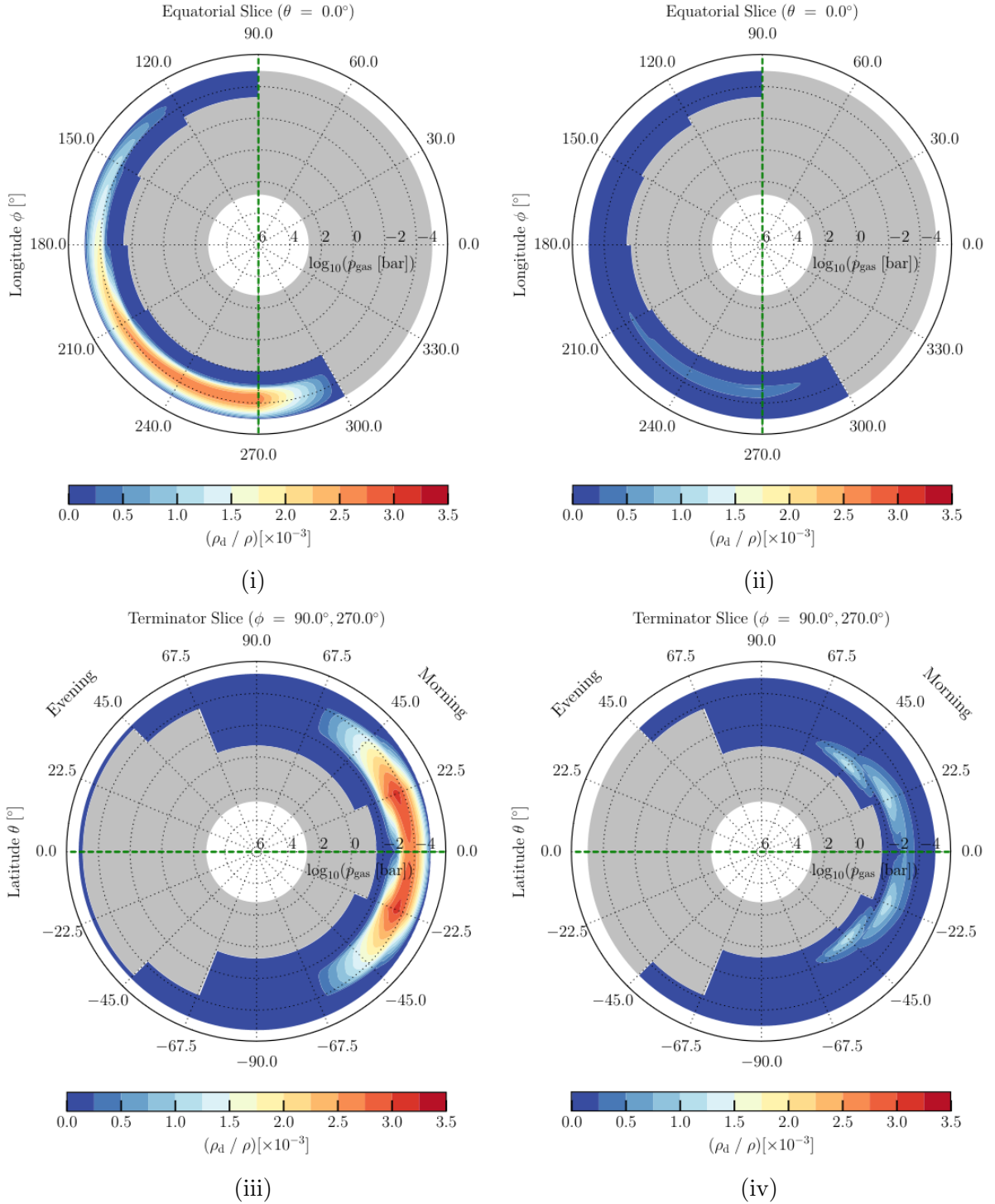


Figure 3.7: Equatorial (top) and terminator (bottom) slice plots of the gas-to-dust ratios in the atmosphere of a planet with the equilibrium temperature $T_{eq} = 2600$ K with normal (left) and scaled mixing (right)

In figure 3.7 the dust-to-gas ratios can be seen. Whereby ρ_d is the particle density and ρ is the general density.

The ratio ranges from 0 to $3.5 \cdot 10^{-3}$ in the normal mixed model and from 0 to 10^{-3} in the scaled mixed model. It is noticeable that it only appears on the night side. Like in the previous shown temperature distribution plot (fig. 3.5), a flow can be detected which proceeds in an anticlockwise manner and again spills over the 270° mark and reaches 300° (fig. 3.7i and fig. 3.7ii). The parameter goes up to a pressure level of 10^{-2} bar, but does not spill over. At the evening terminator the ratio only goes a little bit over 10^{-4} bar into the atmosphere.

The most conspicuous difference between the normal mixed and the scaled mixed one is that the higher ratio in the normal mixed plot is at a pressure level of about 10^{-4} bar. Here the ratio reaches up to $2.5 \cdot 10^{-3}$, while in the scaled mixed plot it only goes up to $1 \cdot 10^{-3}$, which is significantly lower. It should also be mentioned, that the sections with the highest ratio range from 210° to a little bit over 270° .

The highest dust-to-gas ratios are on the morning side with $3.5 \cdot 10^{-3}$ at 22.5° and -22.5° , shown in figure 3.7iii. At the same locations the ratio in the scaled mixed model (fig. 3.7iv) only reaches a value of 10^{-3} . A big portion of the evening side does not have any dust-to-gas ratios.

The normal mixed one reaches a higher dust-to-gas ratio than the scaled mixed one.

Mean particle size

The mean particle size distribution is depicted in figure 3.8, whereby the size is given logarithmic and in $[\mu\text{m}]$. It looks very similar to the dust-to-gas ratio (figure 3.7). As in the previous figure the parameter range only from $\phi = 90^\circ$ to $\phi = 300^\circ$ and likewise reach the highest pressure level of 10^{-2} bar (fig. 3.8i and fig. 3.8ii).

The size of the particle grow with the higher pressure as seen in figure 3.8i. Compared to the size of $10^{-2} \mu\text{m}$ at $p_{gas} = 10^{-4}$ bar, it goes up to $10^{2.5} \mu\text{m}$ at $p_{gas} = 10^{-2}$ bar. While in the right scaled mixed plot this growth is rather less only going up to $10^0 \mu\text{m}$.

The greatest size of $10^4 \mu\text{m}$ is located at the latitudes of 67.5° and -67.5° on the morning side of the planet (fig. 3.8iii). Here it also reaches over 10^{-2} bar.

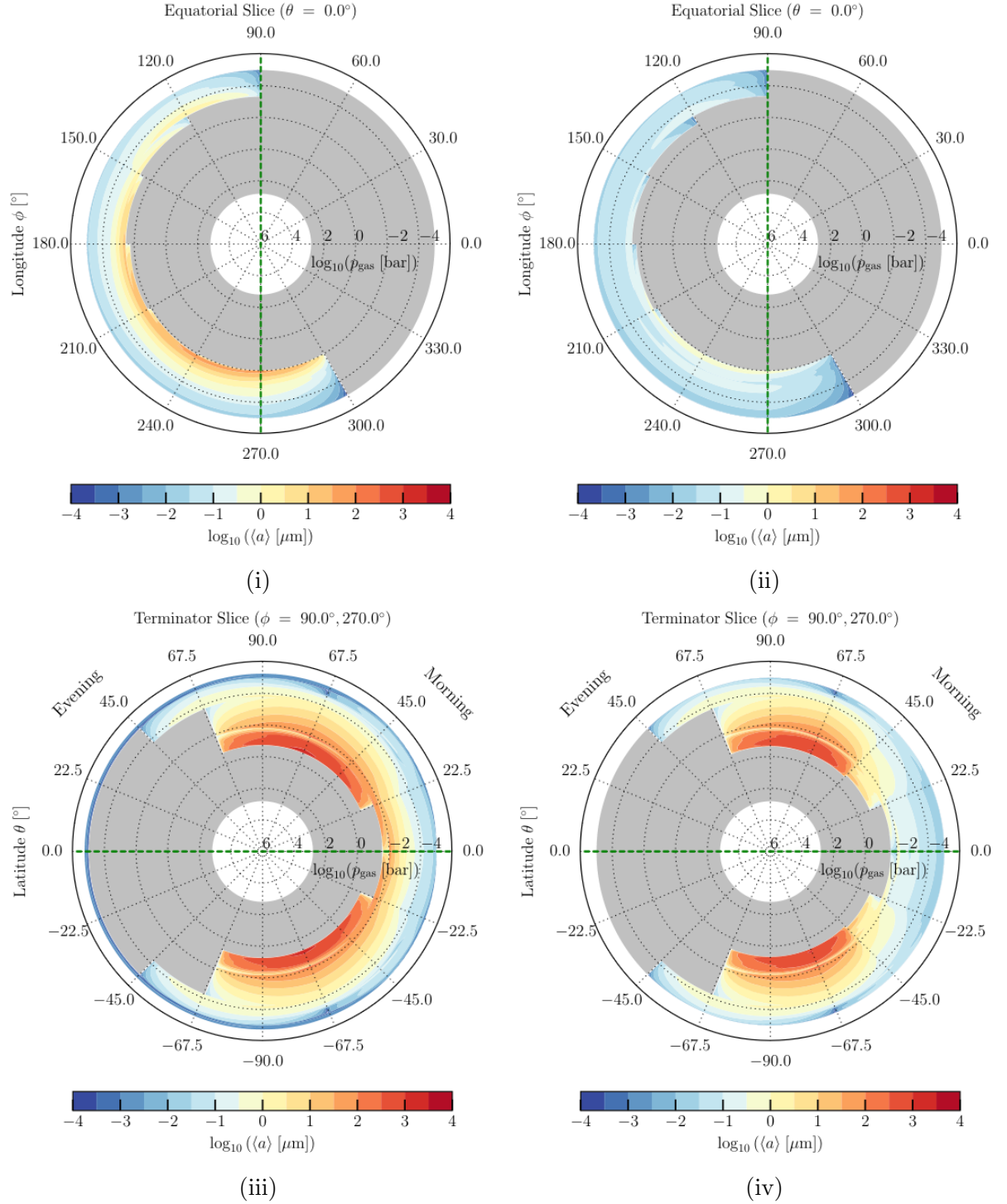


Figure 3.8: Equatorial (top) and terminator (bottom) slice plots of the mean particle size in the atmosphere of a planet with the equilibrium temperature $T_{eq} = 2600$ K with normal (left) and scaled mixing (right)

3.3.2 Planets with an equilibrium temperature of 1800 K

Gas temperature distribution

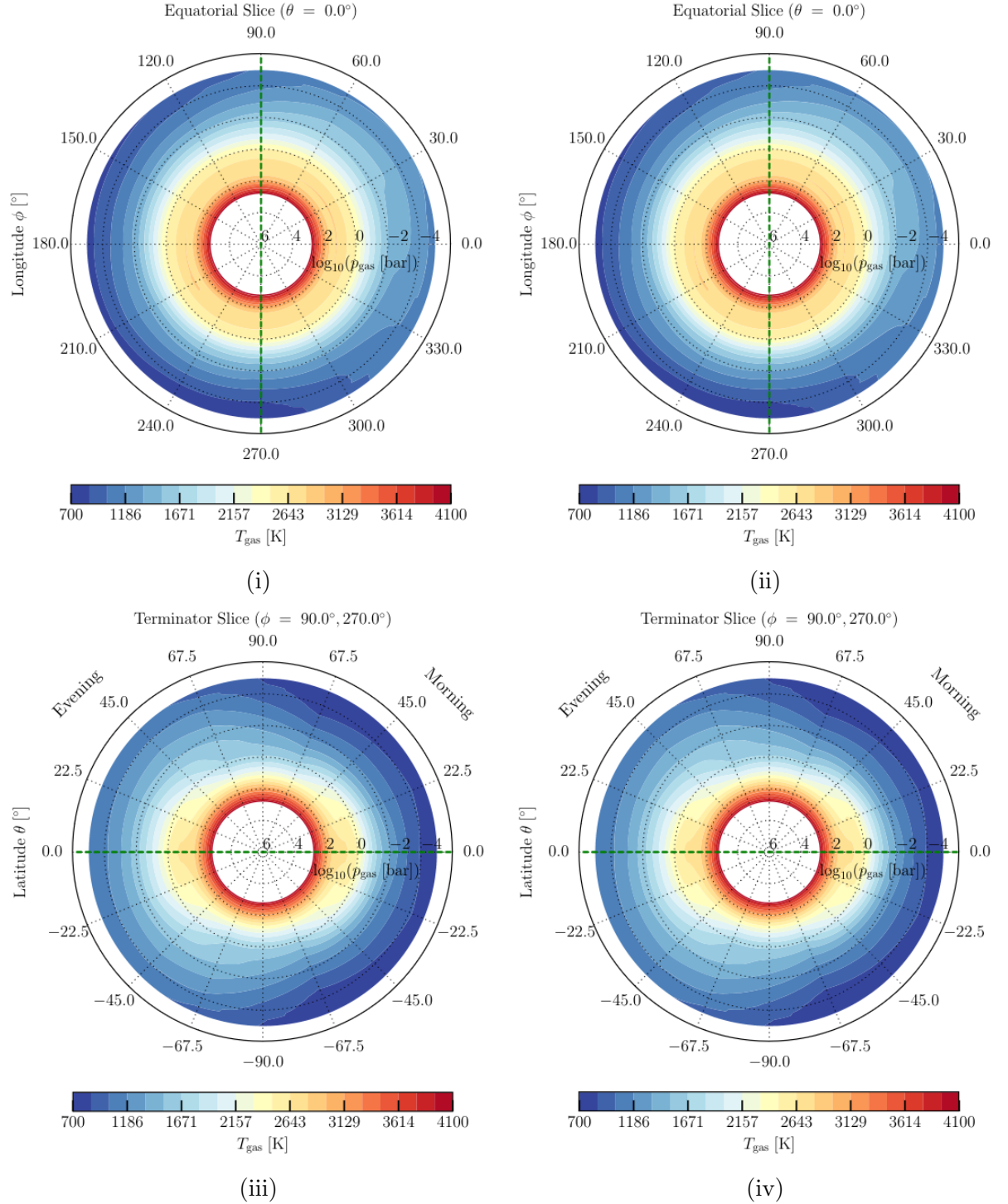


Figure 3.9: Equatorial (top) and terminator (bottom) slice plots of the gas temperature course in the atmosphere of a planet with the equilibrium temperature $T_{eq} = 1800$ K with normal (left) and scaled mixing (right)

The gas temperature distribution in the atmosphere of a $T_{eq} = 1800$ K exoplanet orbiting around a F host star is displayed in figure 3.9. The temperature ranges here from 700 K to 4100 K, whereby the temperature increases the closer it reaches the center and at about 10^3 bar the maximum temperature is reached.

It can be seen that the night side has a less higher temperature than the day side. But the region of higher temperature at 30° , which was seen in the gas temperature distribution of a $T_{eq} = 2600$ K planet (fig. 3.5) does not exist here.

In the terminator slices it can be observed that the morning side is also much cooler than the evening side. With the lowest temperature of 700 K on the morning and 1186 K on the evening side (fig. 3.9iii). In case of the gas temperature distribution there are no differences detected between the normal mixed and the scaled mixed simulations.

Nucleation rate

In the atmosphere of the 1800 K planet nucleation happens on the night and the day side, like shown in the equatorial slice plots in figure 3.10. Between 180° and 330° in the normal mixed plot 3.10i the nucleation reaches to a pressure level of 10^{-2} bar. In the range between 0° and 60° nucleation only reaches 10^{-4} bar. So it can be said that the nucleation reaches a deeper pressure level on the night side than on the day side. In the scaled mixed plot 3.10ii the nucleation does not reach such a deep pressure level and also has a smaller nucleation rate than the normal mixed plot. The scaled mixed model reaches as its highest rate $10^{-4} \text{ cm}^{-3}\text{s}^{-1}$, while the normal mixed model reaches $10^{-2} \text{ cm}^{-3}\text{s}^{-1}$.

It can be seen in the terminator slices that the nucleation on the morning side reaches with the highest pressure level of 10^{-2} bar deeper pressures than on the evening side, where the highest reached pressure lies between 10^{-4} bar and 10^{-3} bar.

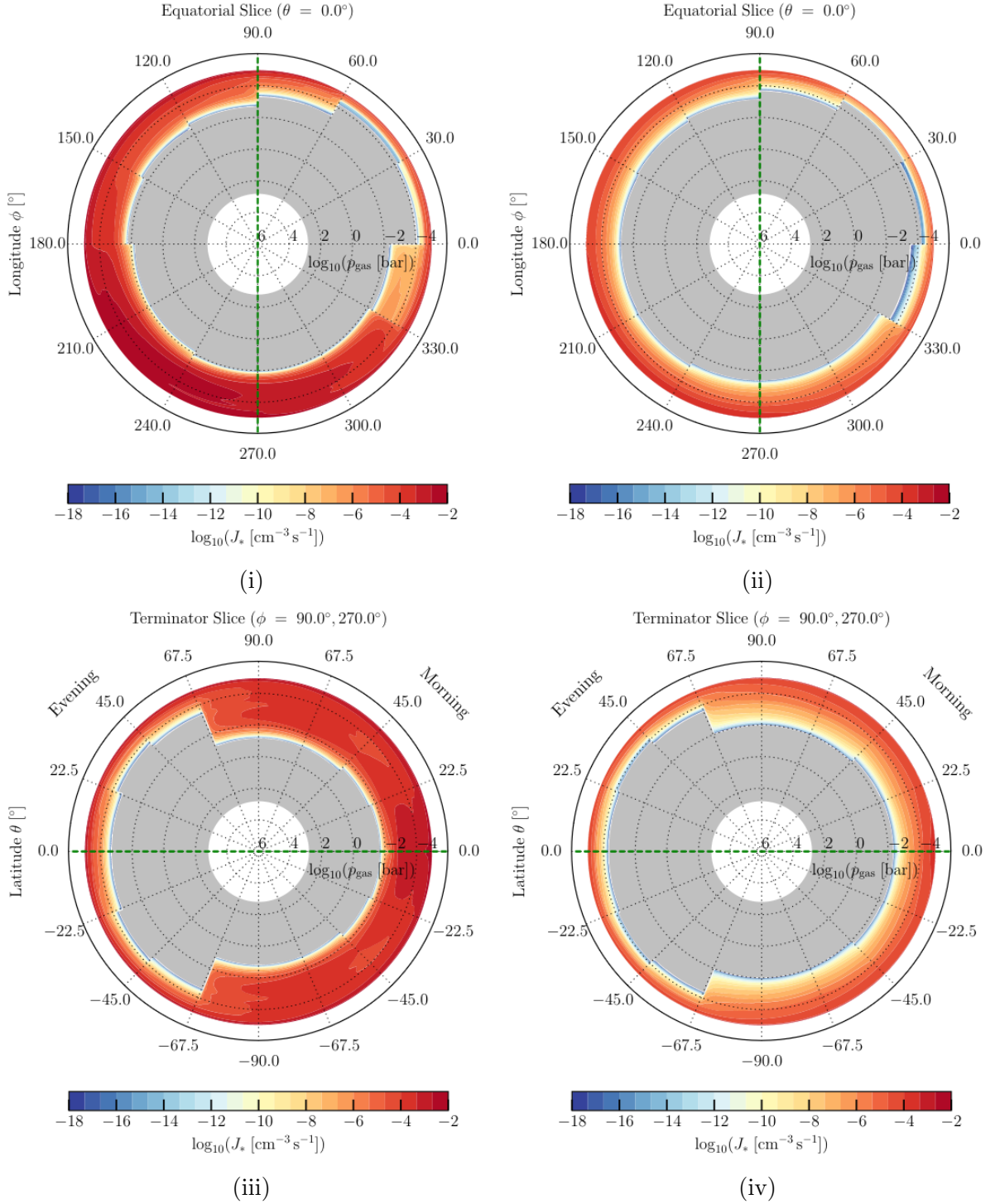


Figure 3.10: Equatorial (top) and terminator (bottom) slice plots of the nucleation rate in the atmosphere of a planet with the equilibrium temperature $T_{eq} = 1800$ K with normal (left) and scaled mixing (right)

Gas-to-dust ratios

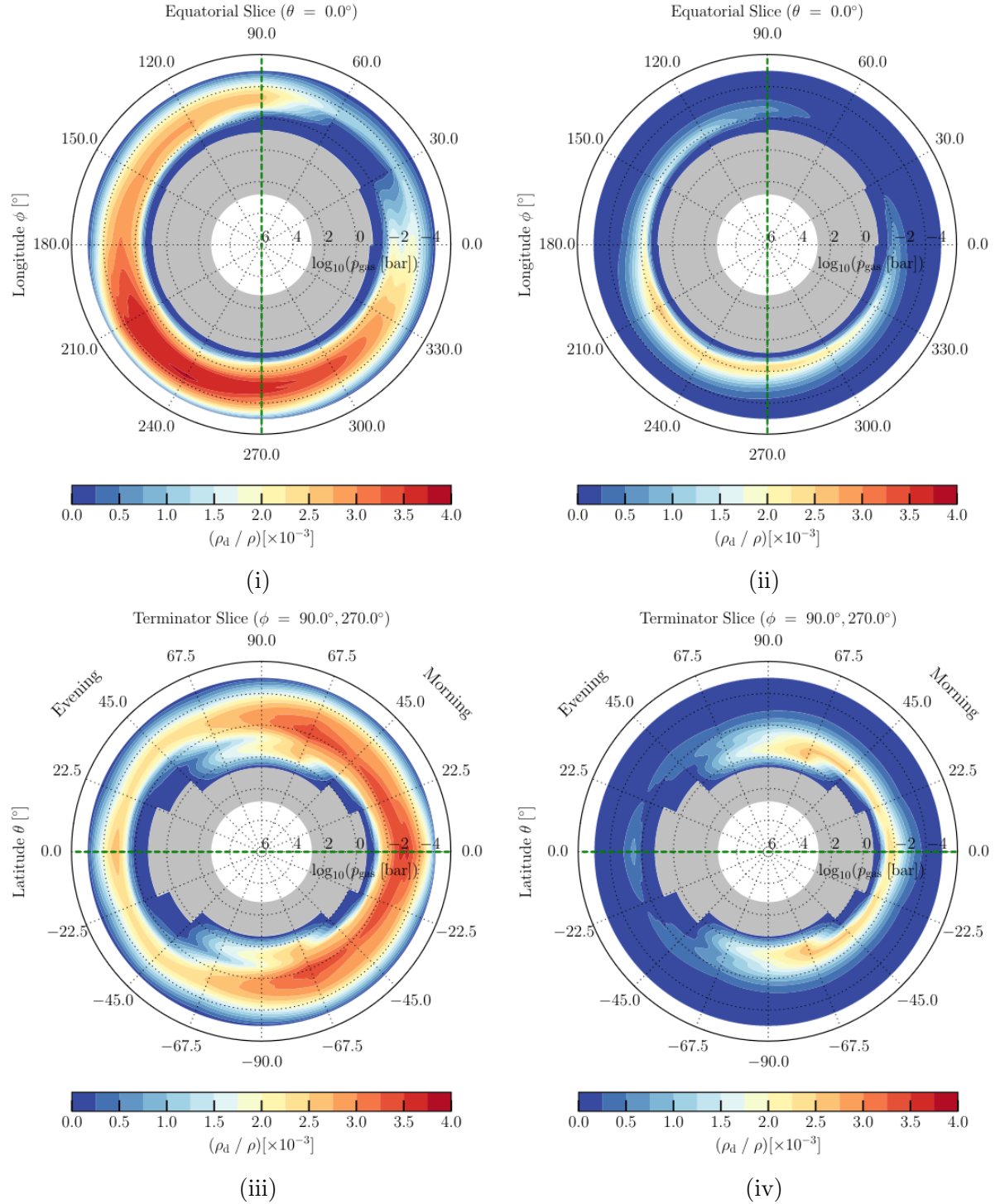


Figure 3.11: Equatorial (top) and terminator (bottom) slice plots of the gas-to-dust ratios in the atmosphere of a planet with the equilibrium temperature $T_{eq} = 1800$ K with normal (left) and scaled mixing (right)

In figure 3.11 the dust-to-gas ratios of a planet with an equilibrium temperature of 1800 K can be seen.

The ration ranges from 0 to 4, but now it appears on both the day and the night side in the equatorial slice. Still there is a higher ratio on the night side, especially on the 240° mark with $4 \cdot 10^{-3}$.

The ratios in the normal mixed slice plot 3.11i reach over 10^{-3} with the highest value of $4 \cdot 10^{-3}$. The scaled mixed plot 3.11ii on the other hand has regions where the ratio is 0, while the highest value reaches only $2.5 \cdot 10^{-3}$ at 210° .

Mean particle size

In figure 3.12 the distribution of the mean particle size on the equatorial and the terminator plane of a planet with $T_{eq} = 1800$ K can be seen.

The values reach from $10^{-2} \mu\text{m}$ to $10^4 \mu\text{m}$ in the normal mixed plot (fig. 3.12i). But the size of the particles in the scaled mixed plot reach only up to $10^{1.5} \mu\text{m}$ (fig. 3.12ii). In both scaled and normal mixed cases the particle size gets bigger the higher the pressure.

In the terminator slice plots it can be seen, that the morning and the evening sides are almost identical structure wise. But still the mean particle size in the scaled mixed version is overall lower than the particle size in the normal mixed version.

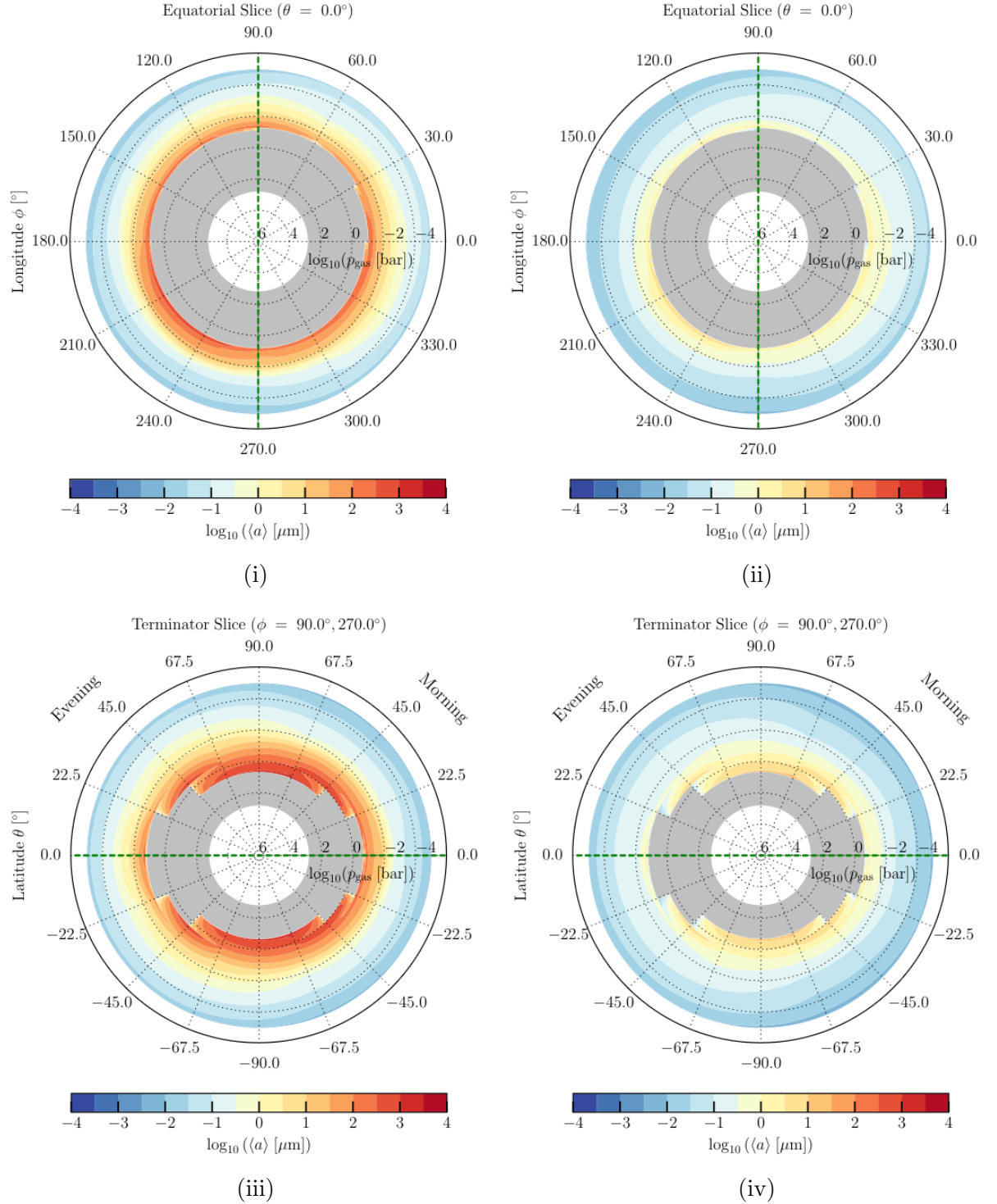


Figure 3.12: Equatorial (top) and terminator (bottom) slice plots of the mean particle size in the atmosphere of a planet with the equilibrium temperature $T_{eq} = 1800$ K with normal (left) and scaled mixing (right)

Chapter 4

Discussion

4.1 Comparison of the GCM models

Figure 3.1 shows the pressure course obtained through an older and a new model of the GCM in dependence of the temperature. Because the calculation of the radiative heating happens outside the older 3D GCM and the material transport is ignored in the equation of the irradiation, the radiative heating and material transport are not well coupled (Baeyens et al., 2022). The night side of the planet is colder than it should be. This shift in temperature can also be seen in the plot in figure 3.1 (dashed lines). The new version of the model has the full radiative transfer calculation inside the model (Schneider et al., 2022). So the computer has to calculate more complex equations, which requires more computational resources and time. But the outcome has a better accuracy of gas phase temperatures (fig. 3.1, solid lines).

4.2 Difference between normal and scaled mixing

All four analysis are performed through normal mixing and scaled mixing. The normal mixing has a multiplication factor of 1, while the scaled mixing has a factor of 10^{-2} . So the normal mixing has a 100 times higher mixing timescale than the scaled mixing, which is why the clouds in the normal mixing slice plots reach deeper into the atmosphere (fig. 3.6 - fig. 3.8 and fig 3.10 - fig. 3.12, right).

The gas temperature distribution does not depend on the mixing timescale. The slice plots are identical (see fig. 3.5 and fig. 3.9). The 10^2 factor difference as well as the identical temperature course are confirmed in the 1D plot of the gas temperature and the mixing timescale in figure 3.2.

In the deeper layers of the atmosphere the particles grow in mass due to surface reactions, which in turn means, that the particle number density there falls. The left graphic in figure 3.3 shows that the particle quantity for normal mixing de-

creases in the deeper atmosphere while the quantity in the scaled mixed version increases a little. With this there must be bigger particles in the deeper layers of the atmosphere for the normal mixing than for the scaled mixing. This agrees with the size curves in the right plot of figure 3.3. This also can be seen in the mean particle slice plots in figure 3.8 and 3.12.

4.3 Intercomparison of planets

Now the previously described slice pots of the two exoplanets with $T_{eq} = 2600$ K and $T_{eq} = 1800$ K will be discussed in the following section.

For a general understanding, the interrelation between the four analyses will be elaborated. According to Helling (2022) the chemical composition of the gas phase, where the seed formation begins, is determined by the gas temperature. This nucleation only happens high up in the atmosphere in a cold environment. Where the nucleation seeds can be formed from the nucleation species (eg. $\text{TiO}_2[\text{s}]$, SiO , NaCl , KCl). Although the seed forming process stops at about 10^{-2} bar (for $T_{eq} = 1800$ K planets) through the atmosphere, cloud particles still gather in deeper layers of the atmosphere. When the seeds-now particles- fall deeper down the atmosphere other material can condensate onto the seed, if the thermal conditions are right. The main particle size grows the deeper the atmosphere, which is nicely shown in the slice plots 3.8 and 3.12. The dust-to-gas ratio is also an indicator where clouds on the planet could be.

From the respective slice plots in subsection 3.3.1 and subsection 3.3.2 it is obvious, that the two exoplanets with various equilibrium temperatures differ from each other. Thou they share the same host star (here F-type). The reason for this lies in the distance of the exoplanet to its host star. So the $T_{eq} = 2600$ K planet is nearer to the star than the $T_{eq} = 1800$ K planet.

The gas temperature distribution of the $T_{eq} = 2600$ K planet (fig. 3.5) shows that the night side is much colder than the day side. This happens because the planet is tidally locked and also very near the star. The cloud particles form on the night side and reach to the day side only on the morning (270°) terminator, not on the evening terminator (90°). The reason behind this is an equatorial jet, which transports cold gas from the night side to the day side. This also explains why the hot region in the equatorial plane is at the 30° mark and not the sub stellar point (0°).

On the $T_{eq} = 1800$ K exoplanet clouds can form on the night and day side. The course of the nuclei (fig. 3.10) confirms this statement. This planet has a larger distance to its host star than the $T_{eq} = 2600$ K planet and is therefore colder. As seen in figure 3.9 the day and night side for this planet are not as distinguishable as the sides of the planet nearer to the star (fig. 3.5). Additionally, due to the cooler temperature the clouds reach deeper into the atmosphere. Due to the further distance to the host star the equatorial jet becomes slower. This agrees with the research of Baeyens et al. (2021), who presents graphics of the zonal winds on different exoplanets (figure 3, page 10).

Chapter 5

Conclusion

The cloud structure in the atmospheres of tidally locked exoplanets with an equilibrium temperature of 1400 K to 2600 K with a F-type host star were simulated. This thesis described and compared the cloud structures of the exoplanets with an equilibrium temperature of 2600 K (near the host star) and 1800 K (further away from the host star). For the modeling the *StaticWeather* model by Woitke and Helling (2003) and the new version of the 3D GCM by Schneider et al. (2022) were used. Emphasis was placed on the used mixing timescale. The scaled mixing with 10^{-2} as a scaling factor and the normal mixing with a factor of 1. Additionally, the new version of the GCM was compared to the older version by Baeyens et al. (2022) by looking at the pressure course of the generated data of the longitudes at 0° , 90° , 180° and -90° . The new version of the GCM is computationally more intensive than the older version. This model takes into account the material transport and calculates the radiative heating inside the GCM. But the comparison between the obtain datasets of the two models show that the new model is more accurate. The results of the here described analysis established the following:

- The reduced mixed model creates a smaller cloud particle number density than the normal mixed model. The mean particle size becomes greater the deeper they are in the atmosphere. Here the size of the particles of the normal mixed version reach higher values than the size of the scaled mixed version. The nucleation also reaches deeper in the atmosphere in the stronger mixed version.
- Exoplanets that are closer to the star have drastic day- night side differences. Because of the tidally locking the day side, which always faces the host star, becomes very hot. The simulation has shown that no clouds can form at such temperatures. So cloud formation only happens on the night side of the planet.
- Exoplanets further away from their host star are more balanced in terms of temperature. Like the simulations have proven that clouds can also form on the day side.

5.1 Outlook

The results of this research provides the cloud formation simulations in atmospheres of hot Jupiters in F star systems with their equilibrium temperature ranging from 1400 K to 2600 K (see section 5.1). The cloud formation modelling in the here used *StaticWeather* model solves the equations of the formation of condensation seeds and the bulk growth of cloud particles. In the future a General Circulation Model could be created in which those equations are directly included. The simulation would take a larger amount of computational resources and time. But with the knowledge of the general cloud structure, a new adapted GCM for exoplanets with F-type host stars could be created. The knowledge about cloud formation in exoplanetary atmospheres can also be used to develop better observation methods for future space missions such as PLATO.

Bibliography

- R. Baeyens, L. Decin, L. Carone, O. Venot, M. Agúndez, and P. Mollière. Grid of pseudo-2D chemistry models for tidally locked exoplanets - I. The role of vertical and horizontal mixing. , 505(4):5603–5653, Aug. 2021. doi: 10.1093/mnras/stab1310.
- R. Baeyens, T. Konings, O. Venot, L. Carone, and L. Decin. Grid of pseudo-2D chemistry models for tidally locked exoplanets - II. The role of photochemistry. , 512(4):4877–4892, June 2022. doi: 10.1093/mnras/stac809.
- L. Carone, R. Baeyens, P. Mollière, P. Barth, A. Vazan, L. Decin, P. Sarkis, O. Venot, and T. Henning. Equatorial retrograde flow in WASP-43b elicited by deep wind jets? , 496(3):3582–3614, Aug. 2020. doi: 10.1093/mnras/staa1733.
- C. Helling. Exoplanet clouds. *Annual Review of Earth and Planetary Sciences*, 47(1):583–606, 2019. doi: 10.1146/annurev-earth-053018-060401. URL <https://doi.org/10.1146/annurev-earth-053018-060401>.
- C. Helling. Clouds in Exoplanetary Atmospheres. In N. Madhusudhan, editor, *ExoFrontiers; Big Questions in Exoplanetary Science*, pages 20–1. 2021. doi: 10.1088/2514-3433/abfa8fch20.
- C. Helling. Cloud formation in Exoplanetary Atmospheres. *arXiv e-prints*, art. arXiv:2205.00454, May 2022. doi: 10.48550/arXiv.2205.00454.
- C. Helling and P. Woitke. Dust in brown dwarfs. V. Growth and evaporation of dirty dust grains. , 455(1):325–338, Aug. 2006. doi: 10.1051/0004-6361:20054598.
- C. Helling, P. Woitke, and W. F. Thi. Dust in brown dwarfs and extra-solar planets. I. Chemical composition and spectral appearance of quasi-static cloud layers. , 485(2):547–560, July 2008. doi: 10.1051/0004-6361:20078220.
- C. Helling, D. Samra, D. Lewis, R. Calder, G. Hirst, P. Woitke, R. Baeyens, L. Carone, O. Herbort, and K. L. Chubb. Exoplanet weather and climate regimes with clouds and thermal ionospheres. A model grid study in support of large-scale observational campaigns. , 671:A122, Mar. 2023. doi: 10.1051/0004-6361/202243956.
- D. D. B. Koll. A Scaling for Atmospheric Heat Redistribution on Tidally Locked Rocky Planets. , 924(2):134, Jan. 2022. doi: 10.3847/1538-4357/ac3b48.

-
- A. D. Schneider, L. Carone, L. Decin, U. G. Jørgensen, P. Mollière, R. Baeyens, S. Kiefer, and C. Helling. Exploring the deep atmospheres of HD 209458b and WASP-43b using a non-gray general circulation model. , 664:A56, Aug. 2022. doi: 10.1051/0004-6361/202142728.
- P. Woitke and C. Helling. Dust in brown dwarfs. II. The coupled problem of dust formation and sedimentation. , 399:297–313, Feb. 2003. doi: 10.1051/0004-6361:20021734.
- P. Woitke and C. Helling. Dust in brown dwarfs. III. Formation and structure of quasi-static cloud layers. , 414:335–350, Jan. 2004. doi: 10.1051/0004-6361:20031605.

Appendix

Comparison of the two GCM models

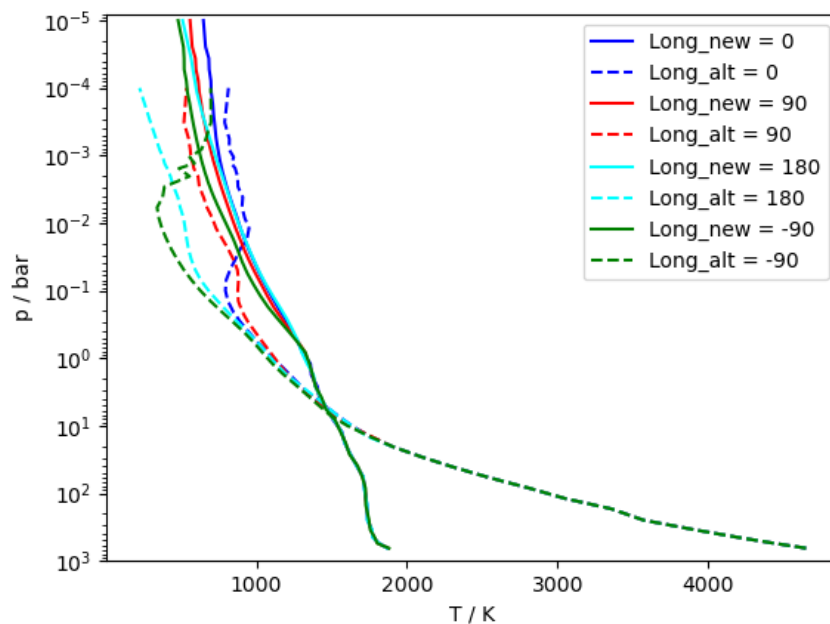


Figure 5.1: The Comparison between two 3D GCM simulations for a planet of $T_{eq} = 1000$ K orbiting an F-type host star: The older simulation model by Bayens (dashed lines) and the new model by Schneider (solid lines) depicted at the sub stellar point (0°), evening terminator (90°), anti stellar point (180°) and at the morning terminator (-90°)

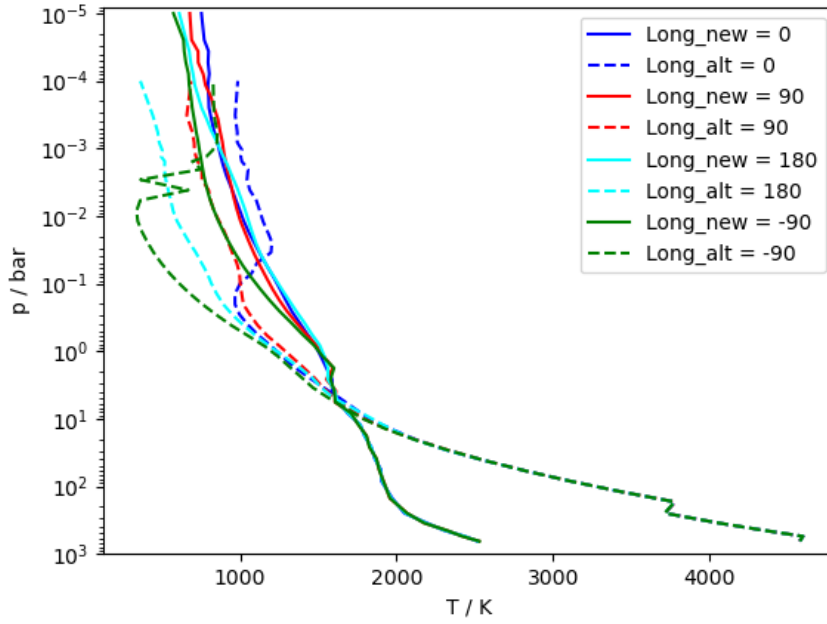


Figure 5.2: The Comparison between two 3D GCM simulations for a planet of $T_{eq} = 1200$ K orbiting an F-type host star: The older simulation model by Bayens (dashed lines) and the new model by Schneider (solid lines) depicted at the sub stellar point (0°), evening terminator (90°), anti stellar point (180°) and at the morning terminator (-90°)

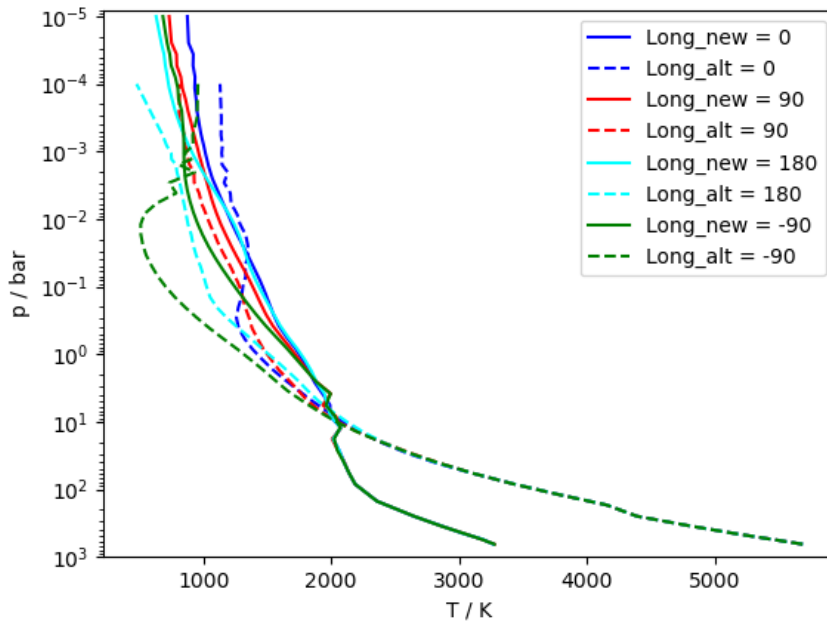


Figure 5.3: The Comparison between two 3D GCM simulations for a planet of $T_{eq} = 1400$ K orbiting an F-type host star: The older simulation model by Bayens (dashed lines) and the new model by Schneider (solid lines) depicted at the sub stellar point (0°), evening terminator (90°), anti stellar point (180°) and at the morning terminator (-90°)

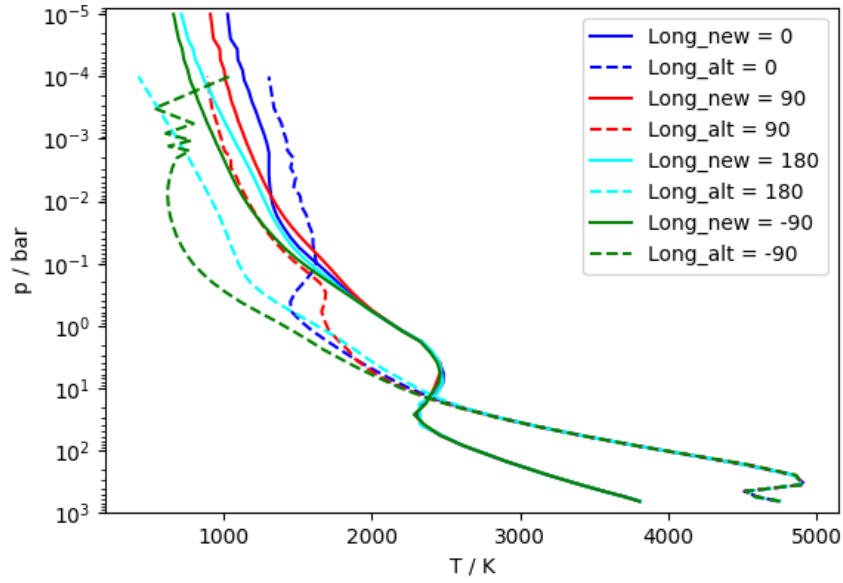


Figure 5.4: The Comparison between two 3D GCM simulations for a planet of $T_{eq} = 1600$ K orbiting an F-type host star: The older simulation model by Bayens (dashed lines) and the new model by Schneider (solid lines) depicted at the sub stellar point (0°), evening terminator (90°), anti stellar point (180°) and at the morning terminator (-90°)

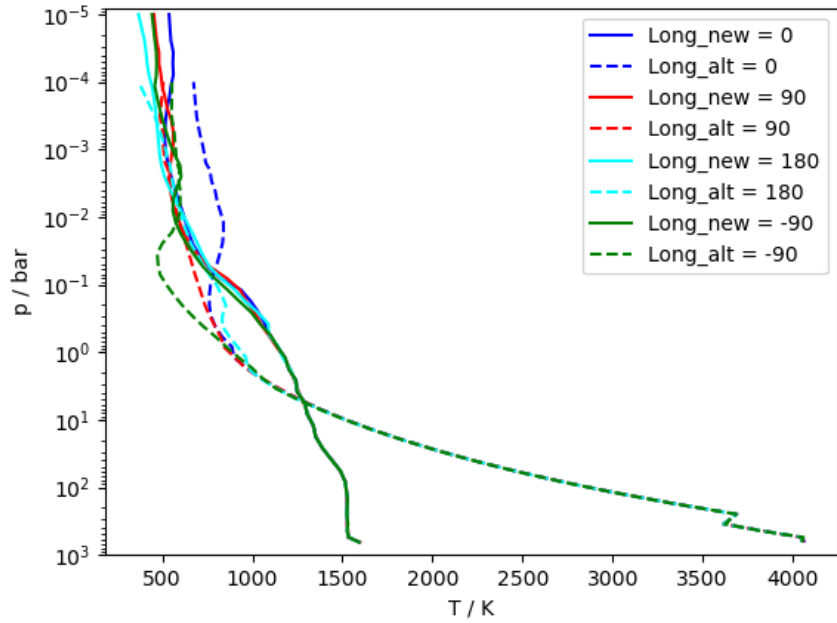


Figure 5.5: The Comparison between two 3D GCM simulations for a planet of $T_{eq} = 1800$ K orbiting an F-type host star: The older simulation model by Bayens (dashed lines) and the new model by Schneider (solid lines) depicted at the sub stellar point (0°), evening terminator (90°), anti stellar point (180°) and at the morning terminator (-90°)

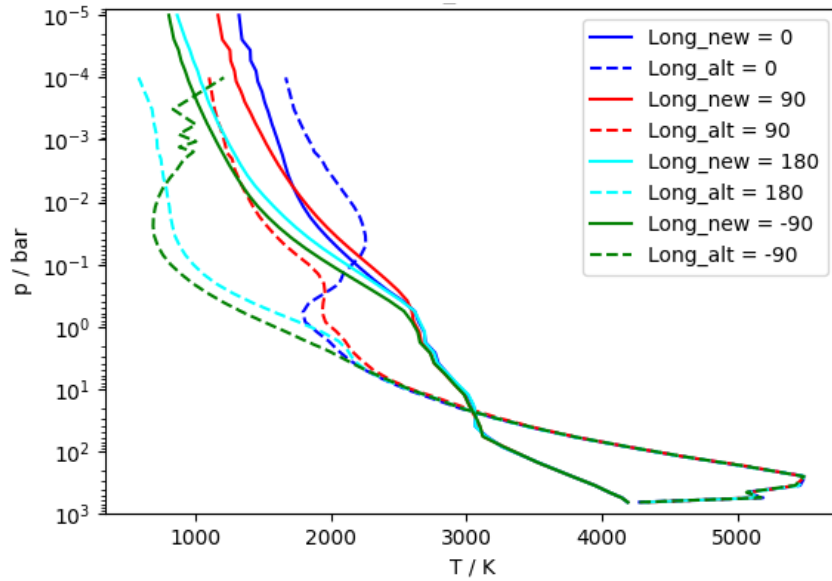


Figure 5.6: The Comparison between two 3D GCM simulations for a planet of $T_{eq} = 2000$ K orbiting an F-type host star: The older simulation model by Bayens (dashed lines) and the new model by Schneider (solid lines) depicted at the sub stellar point (0°), evening terminator (90°), anti stellar point (180°) and at the morning terminator (-90°)

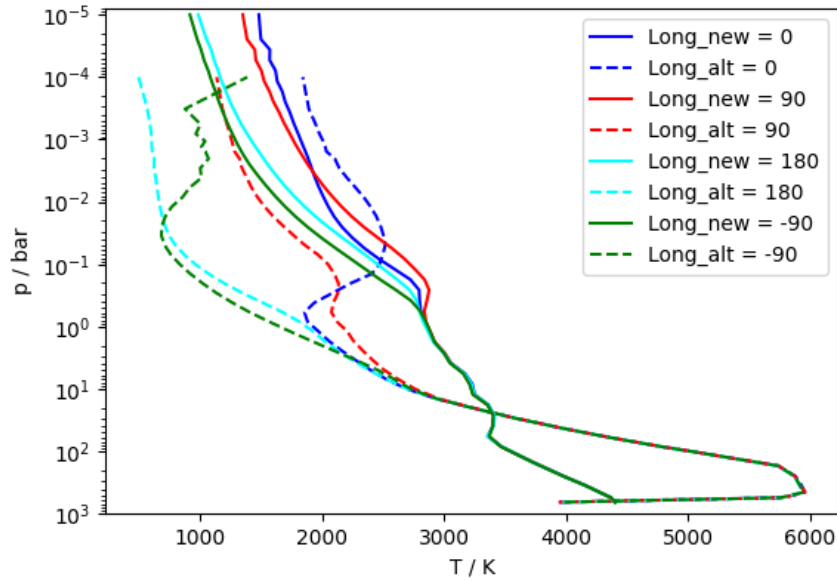


Figure 5.7: The Comparison between two 3D GCM simulations for a planet of $T_{eq} = 2200$ K orbiting an F-type host star: The older simulation model by Bayens (dashed lines) and the new model by Schneider (solid lines) depicted at the sub stellar point (0°), evening terminator (90°), anti stellar point (180°) and at the morning terminator (-90°)

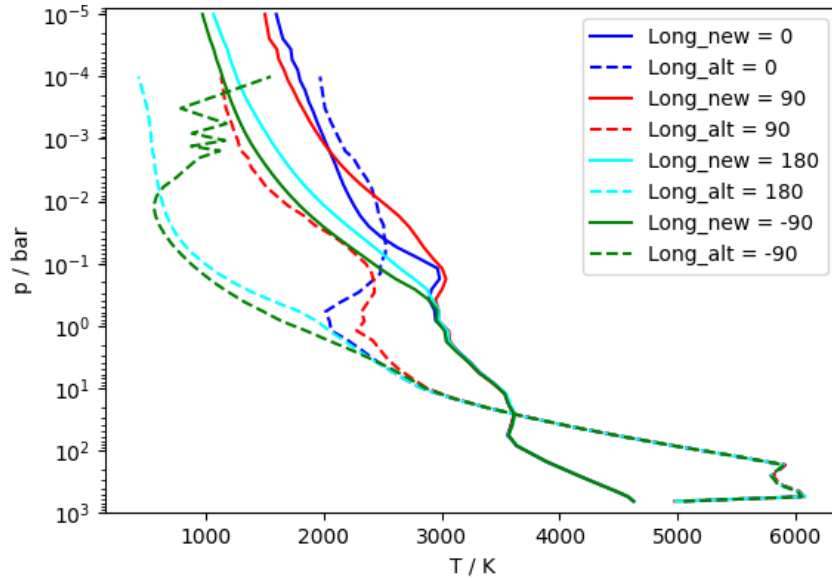


Figure 5.8: The Comparison between two 3D GCM simulations for a planet of $T_{eq} = 2400$ K orbiting an F-type host star: The older simulation model by Bayens (dashed lines) and the new model by Schneider (solid lines) depicted at the sub stellar point (0°), evening terminator (90°), anti stellar point (180°) and at the morning terminator (-90°)

Comparison of scaled and normal mixing

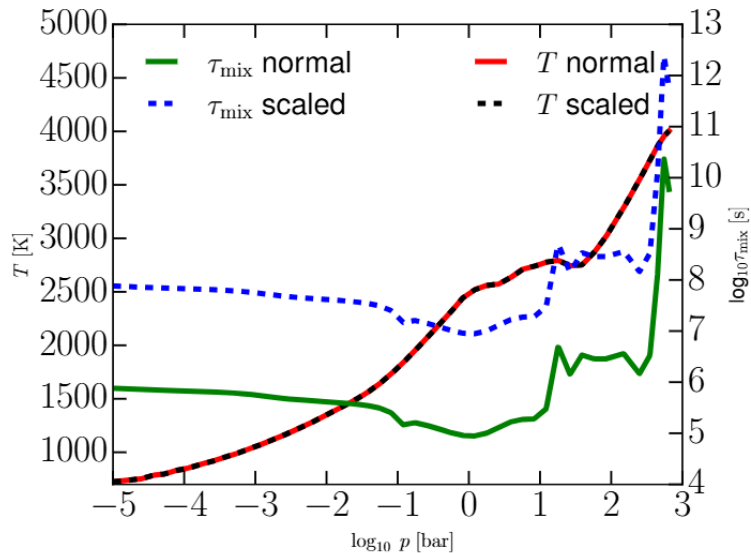


Figure 5.9: The gas temperature T_{gas} [K] and the mixing timescale τ_{mix} [s] for the normal (solid line) and the scaled mixing (dashed line) in dependence of the gas pressure p_{gas} [bar] for an exoplanet with an equilibrium temperature of 1800 K

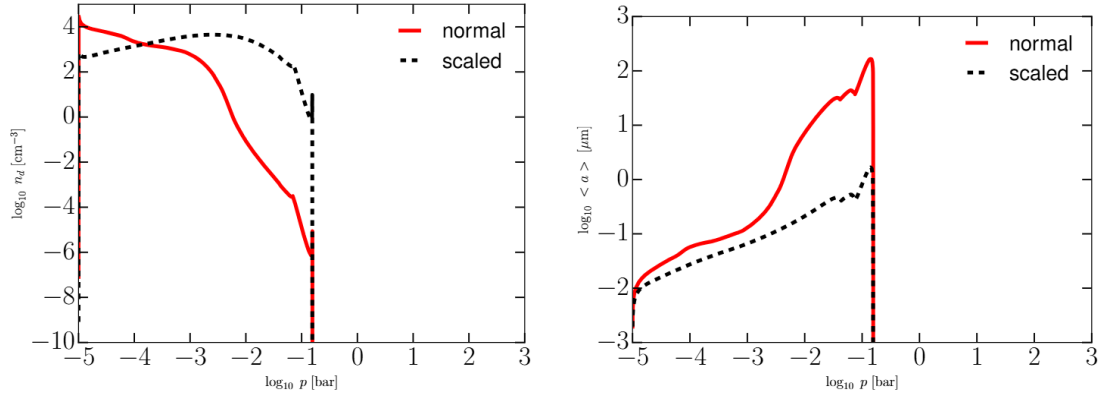


Figure 5.10: The cloud particle number density n_d [cm^{-3}] (left) and the mean particle size $\langle a \rangle$ [μm] (right) for the normal (solid line) and the reduced mixing (dashed line) in dependence of the gas pressure p_{gas} [bar] for an exoplanet with an equilibrium temperature of 1800 K

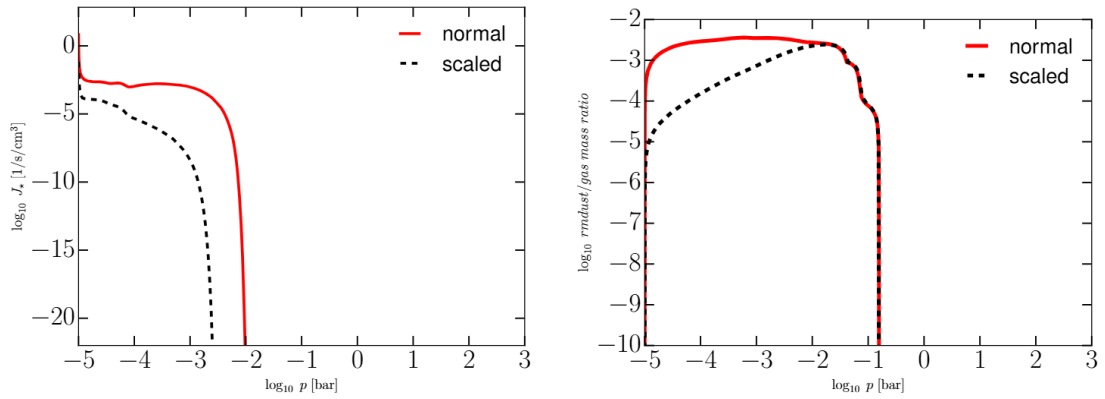


Figure 5.11: The nucleation rate J_* [$\text{cm}^{-3}\text{s}^{-1}$] (left) and the dust-to-gas ratio ρ_{dust}/ρ_{gas} (right) for the normal (solid line) and the scaled mixing (dashed line) in dependence of the gas pressure p_{gas} [bar] for an exoplanet with an equilibrium temperature of 1800 K

Simulations of the cloud structure

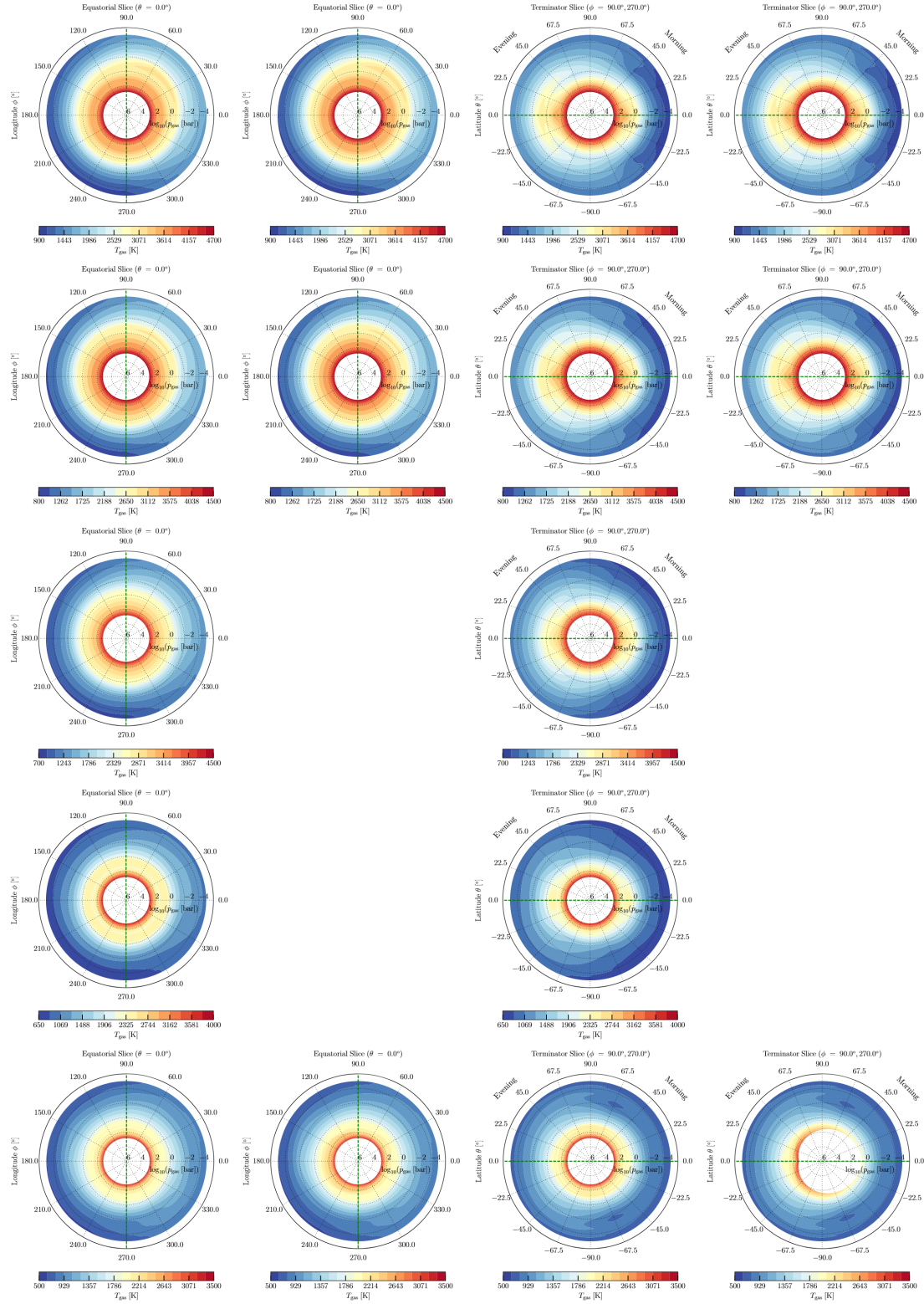


Figure 5.12: Gas temperature distribution left to right: equatorial slice plot with normal mixing, equatorial slice plot with scaled mixing, terminator slice plot with normal mixing, terminator slice plot with scaled mixing; top to bottom: $T_{eq} = 2400$ K, $T_{eq} = 2200$ K, $T_{eq} = 2000$ K, $T_{eq} = 1600$ K, $T_{eq} = 1400$ K; (In terminator slice of $T_{eq} = 1400$ K one profile is missing)

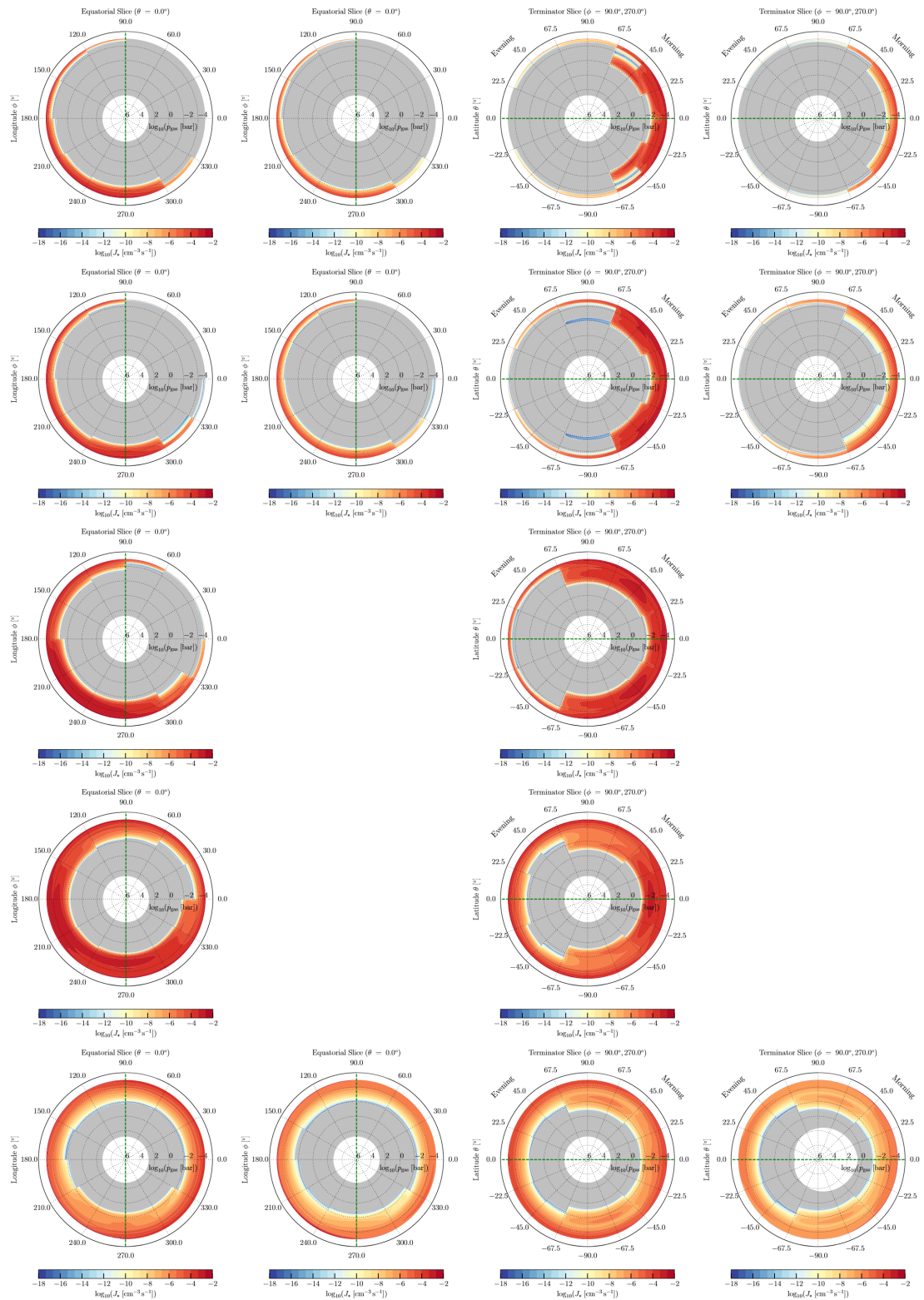


Figure 5.13: Nucleation rate:
left to right: equatorial slice plot with normal mixing, equatorial slice plot with scaled mixing, terminator slice plot with normal mixing, terminator slice plot with scaled mixing;
top to bottom: $T_{eq} = 2400$ K, $T_{eq} = 2200$ K, $T_{eq} = 2000$ K, $T_{eq} = 1600$ K, $T_{eq} = 1400$ K; (In terminator slice of $T_{eq} = 1400$ K one profile is missing)

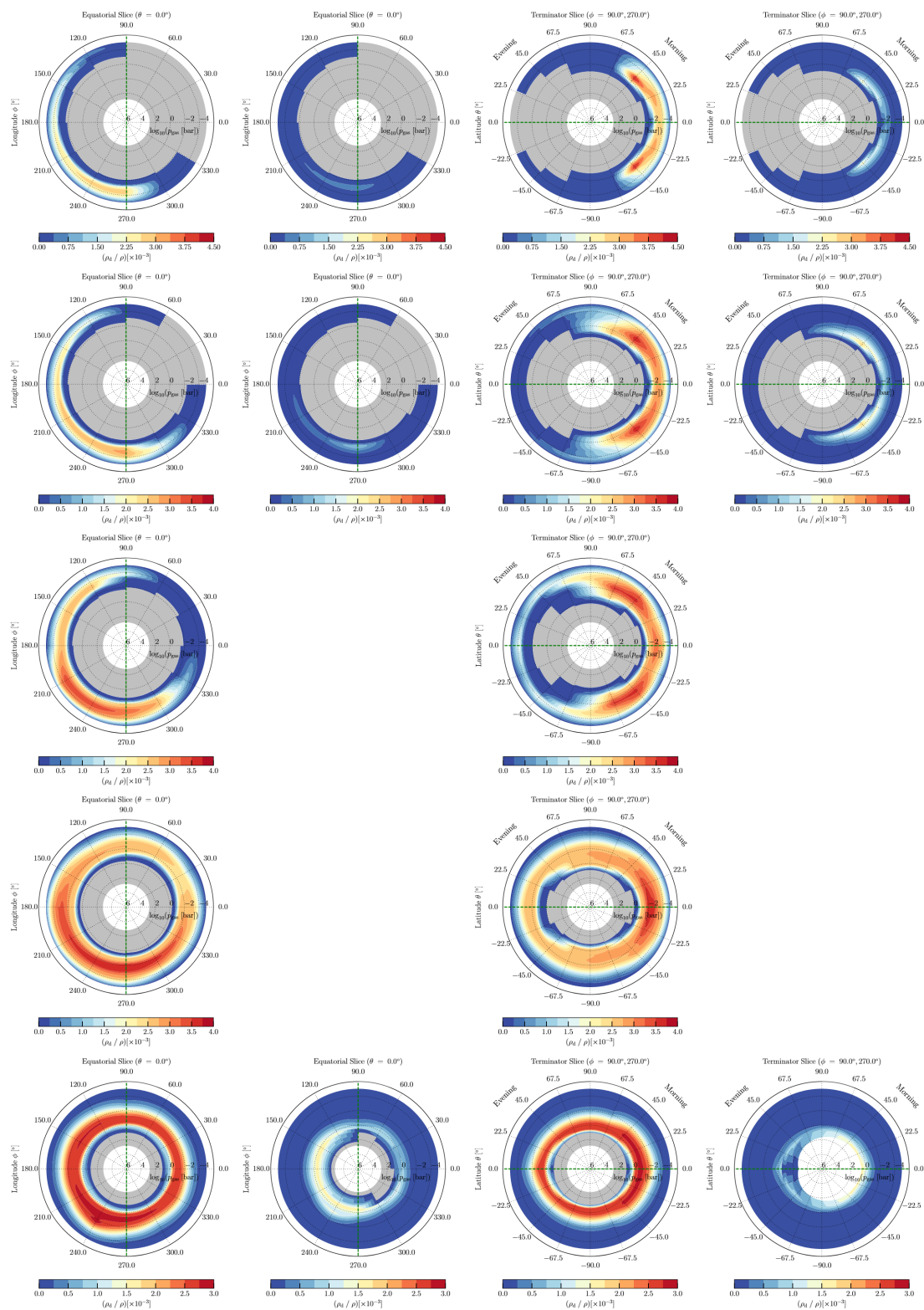


Figure 5.14: Gas-to-dust ratio:

left to right: equatorial slice plot with normal mixing, equatorial slice plot with scaled mixing, terminator slice plot with normal mixing, terminator slice plot with scaled mixing;

top to bottom: $T_{eq} = 2400$ K, $T_{eq} = 2200$ K, $T_{eq} = 2000$ K, $T_{eq} = 1600$ K, $T_{eq} = 1400$ K; (In terminator slice of $T_{eq} = 1400$ K one profile is missing)

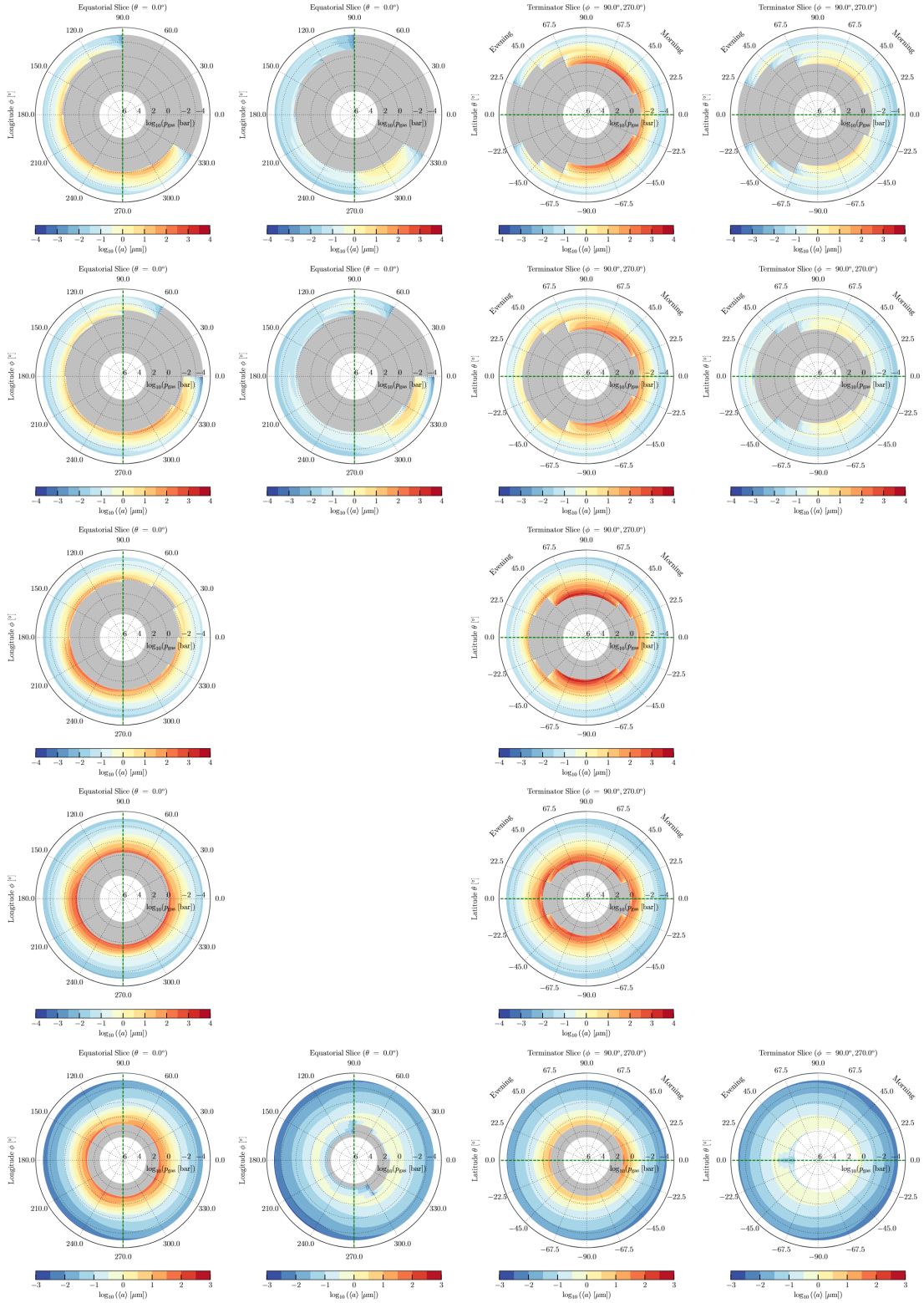


Figure 5.15: Mean particle size; left to right: equatorial slice plot with normal mixing, equatorial slice plot with scaled mixing, terminator slice plot with normal mixing, terminator slice plot with scaled mixing; top to bottom: $T_{eq} = 2400$ K, $T_{eq} = 2200$ K, $T_{eq} = 2000$ K, $T_{eq} = 1600$ K, $T_{eq} = 1400$ K; (In terminator slice of $T_{eq} = 1400$ K one profile is missing)

Declaration

I declare that I have authored this thesis independently, that I have not used other than the declared sources/resources, and that I have explicitly indicated all material which has been quoted either literally or by content from the sources used. The text document uploaded to UNIGRAZonline or TUGRAZonline is identical to the present bachelor's thesis.

Graz, July 7, 2024